"An eiganstrain analysis of mechanical properties of nanostructured ceramic coatings by synchrotron probe"

Thomas Tsakalakos

Dept. of Materials Science and Engineering, Rutgers University
M. Croft[1] , Physics Dept., Rutgers University

K. Akdogan, A. Ignatov, N. Ahmedi, L. Balarinni, J. Giminez, M. McNeley,[1]

Zhong[2], N. Jisrawi[3], J. Skaritka[2], N. Simos[2],T. Fast[3], R. Sadangi[3], V. Shukla[3]

[1]Department of Physics, Rutgers University, Piscataway, NJ 08854;
[2]National Synchrotron Light Source, Brookhaven National Laboratory, Upton, NY; 11973
[3]Mat Sc & Eng. Dept, Rutgers University, Piscataway, NJ; 08854
[4] Naval Research Laboratory, 4555 Overlook Ave., SW, Washington, DC 20375

L. Kabacoff Office of Naval Research
G. Kim, Perpetual Technologies, Canada
E. Lavernia University of California, Davis
R. Rigney A&A INc , S. Brunswick NJ
K. Scandell MT NAVSEA

Brookhaven National
Synchrotron Light Source X-17B1

We acknowledge the support of the Office of Naval Research under grant N00014-02-1-0772.

Report Documentation Page

Form Approved
OMB No. 0704-0188

1. REPORT DATE **JUN 2010**	2. REPORT TYPE **N/A**	3. DATES COVERED **-**

4. TITLE AND SUBTITLE **An eiganstrain analysis of mechanical properties of nanostructured ceramic coatings by synchrotron probe**	5a. CONTRACT NUMBER 5b. GRANT NUMBER 5c. PROGRAM ELEMENT NUMBER
6. AUTHOR(S)	5d. PROJECT NUMBER 5e. TASK NUMBER 5f. WORK UNIT NUMBER
7. PERFORMING ORGANIZATION NAME(S) AND ADDRESS(ES) **Dept. of Materials Science and Engineering, Rutgers University**	8. PERFORMING ORGANIZATION REPORT NUMBER
9. SPONSORING/MONITORING AGENCY NAME(S) AND ADDRESS(ES)	10. SPONSOR/MONITOR'S ACRONYM(S) 11. SPONSOR/MONITOR'S REPORT NUMBER(S)

12. DISTRIBUTION/AVAILABILITY STATEMENT
Approved for public release, distribution unlimited

13. SUPPLEMENTARY NOTES
See also ADM002307. ECI International Conference on Sub-Micron and Nanostructured Ceramics Held in Colorado Springs, Colorado on 7-12 June 2009, The original document contains color images.

14. ABSTRACT

15. SUBJECT TERMS

16. SECURITY CLASSIFICATION OF:			17. LIMITATION OF ABSTRACT	18. NUMBER OF PAGES	19a. NAME OF RESPONSIBLE PERSON
a. REPORT	b. ABSTRACT	c. THIS PAGE			
unclassified	**unclassified**	**unclassified**	**UU**	**54**	

Standard Form 298 (Rev. 8-98)
Prescribed by ANSI Std Z39-18

Outline

- Introductory Remarks
- Residual Stresses
- Synchrotron EDXRD Strain & Phase Mapping
- Thermal Sprayed Nanostructured Coatings
- In situ four-point bending experiments
- Eigenstrain Analysis
- Reliable Life prediction
- Applications to Engineering Systems

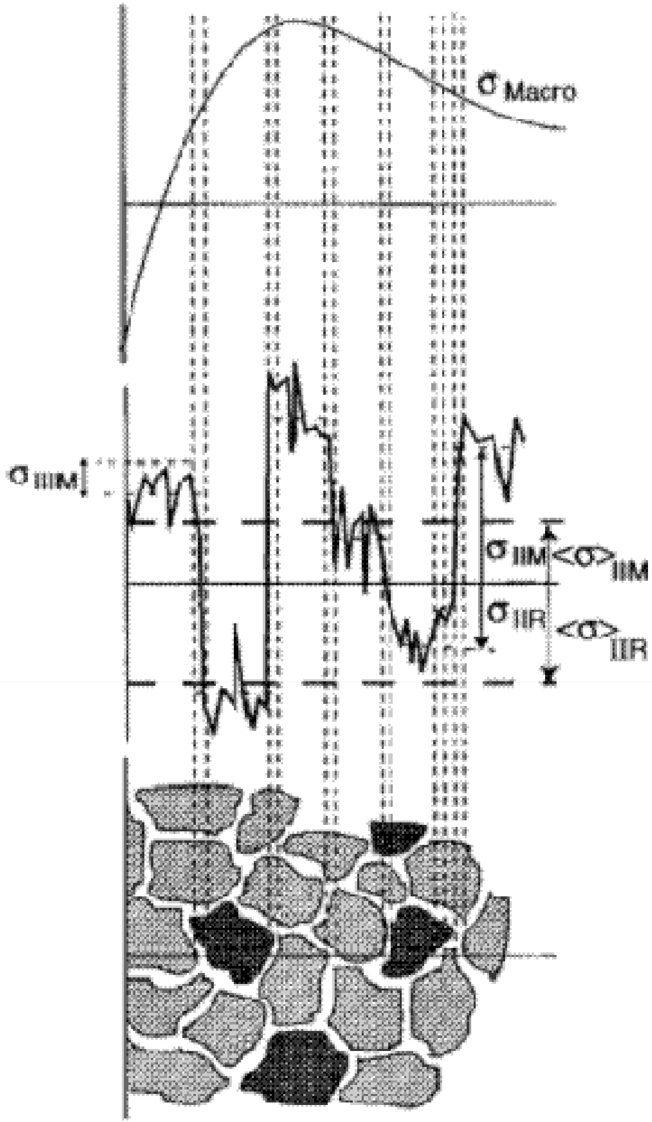

M and R denote matrix and reinforcement respectively

2 Residual stress fields can be categorised according to characteristic length scales $l_{0,I}$, $l_{0,II}$, and $l_{0,III}$ over which they self-equilibrate: for type I, $l_{0,I}$ represents considerable fraction of component; for type II, $l_{0,II}$ is comparable to grain dimensions, while for type III, $l_{0,III}$ is less than grain diameter

TYPE OF RESIDUAL STRESSES MEASURED BY EDXRD

Type I σ_I Macroscale
Type II σ_{II} Mesoscale
Type III σ_{III} Nanoscale

For a two phase material, the macrostress σ_I (type I) is continuous across phases, but the type II and III stresses are not. As a result, even when the sampling area is greater than the characteristic areas for type σ_{II} II and type σ_{III} III, non-zero phase-average microstresses can be recorded. Considering the stresses in two phases:

$0=f\langle\sigma_\alpha\rangle^{II}+(1-f)\langle\sigma_\beta\rangle^{II}$ where f is the volume fracrion of phase α.

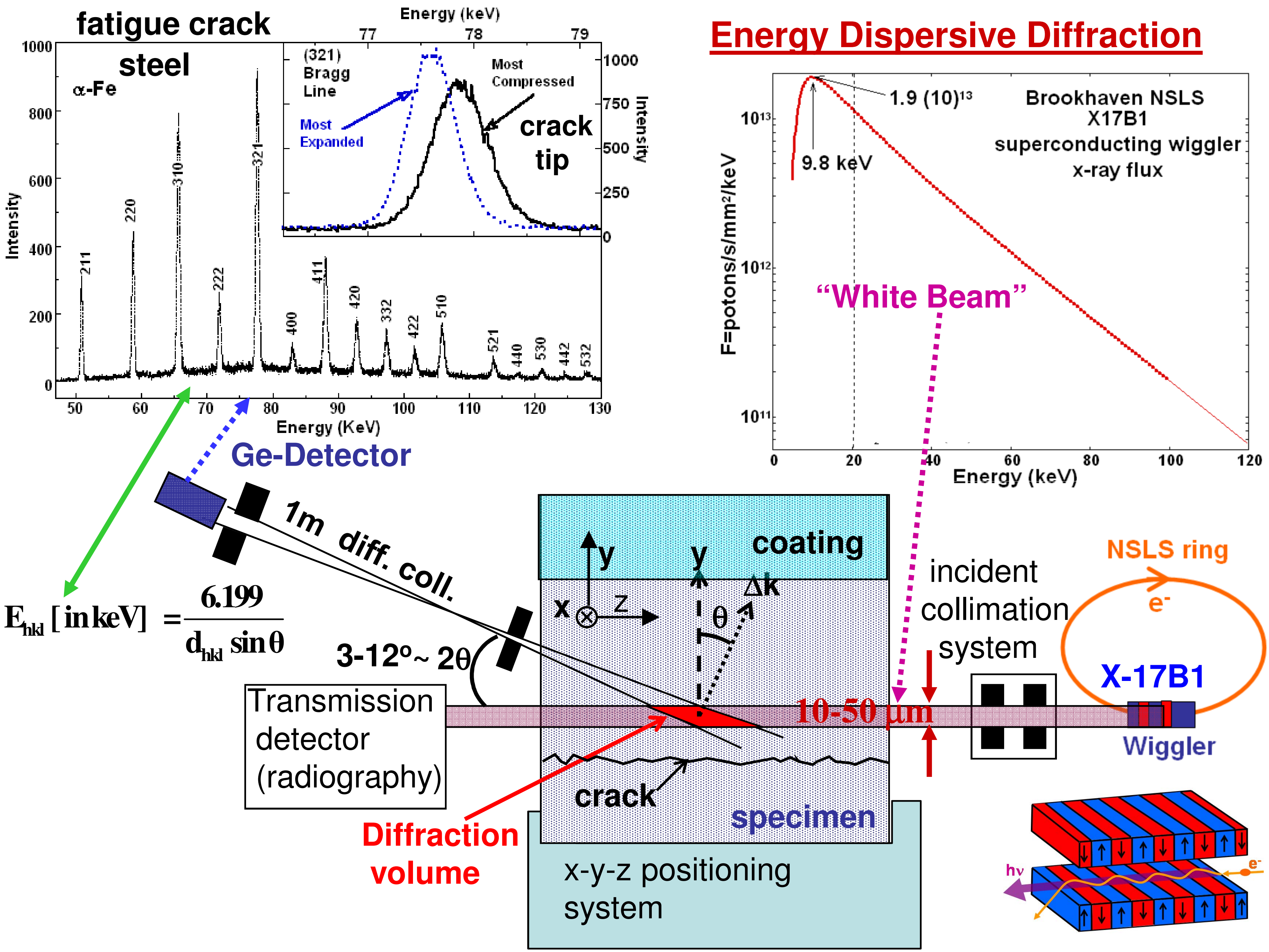

fatigue crack
steel
α-Fe
Intensity
Energy (KeV)
Energy (keV)
(321)
Bragg
Line
Most
Expanded
Most
Compressed
crack
tip
Intensity
Energy Dispersive Diffraction
1.9 (10)13
9.8 keV
Brookhaven NSLS
X17B1
superconducting wiggler
x-ray flux
F=potons/s/mm²/keV
"White Beam"
Energy (keV)
Ge-Detector
1m diff. coll.
$E_{hkl}\,[\text{in keV}] = \dfrac{6.199}{d_{hkl}\sin\theta}$
3-12° ~ 2θ
Transmission
detector
(radiography)
coating
incident
collimation
system
NSLS ring
e-
X-17B1
10-50 μm
Wiggler
crack
specimen
Diffraction
volume
x-y-z positioning
system
hν

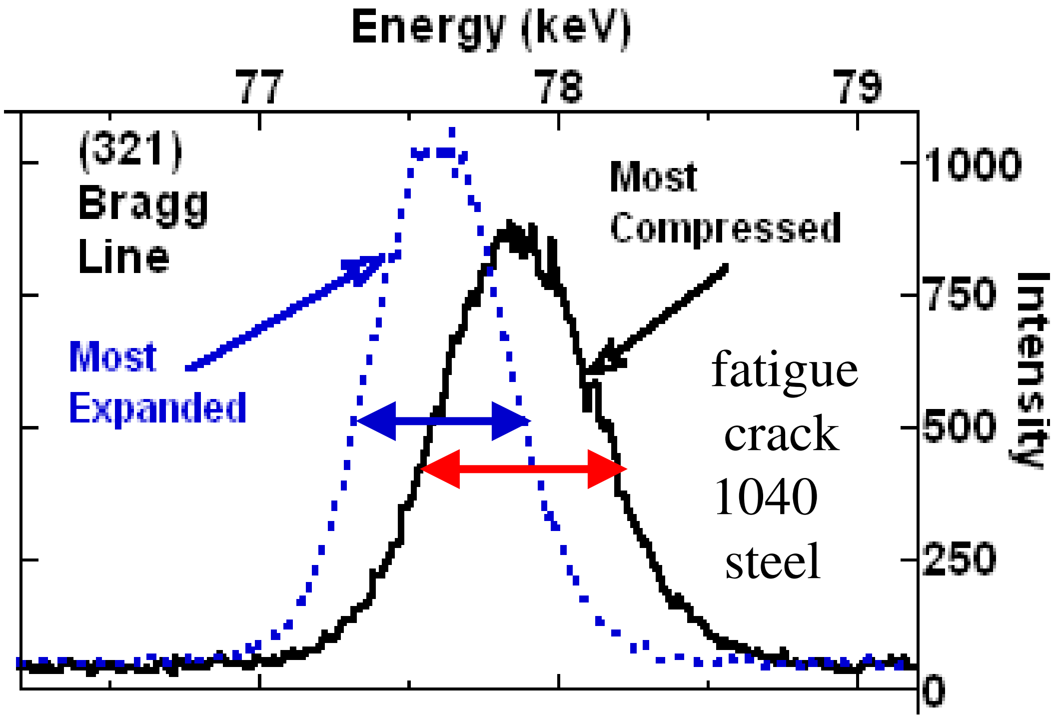

EDXRD Bragg Line Width

$$E_{hkl}\,[\text{in keV}] = \frac{b}{d_{hkl}\sin\theta}$$

$$b = 6.199\,[\text{keV}\,(\mathring{A})]$$

Assume Gaussian fitting

$$(\delta E)^2 = (\delta E_{det})^2 + (\delta E_{gs})^2 + (\delta E_{ms})^2$$

radioactive & atomic florescence standards

$$\delta E_{det} = \frac{a}{E}$$

coherent scattering domain (<~grain) size

Debye-Sherrer

$$(\delta E_{gs})^2 = \left(\frac{bK}{d_{gs}\sin(\theta)}\right)^2$$

K~0.9

micro-strain

$$\delta E_{ms} = 2e\,E$$

standards

- d_o values to determine strains.
- How:
  - Find regions with Stress-free
  - Find samples of Stress-free
  - Use powders
  - Use of equilibrium conditions:
    - Multi phases
    - Force/moment balance

Constitutive equation

$$\sigma_{ij} = \frac{E}{1+\nu}\left[\varepsilon_{ij} + \delta_{ij}\left(\frac{\nu}{1-2\nu}\right)(\varepsilon_{11} + \varepsilon_{22} + \varepsilon_{33})\right]$$

In-Situ Study of the Development of Intergranular/Interphase Strains

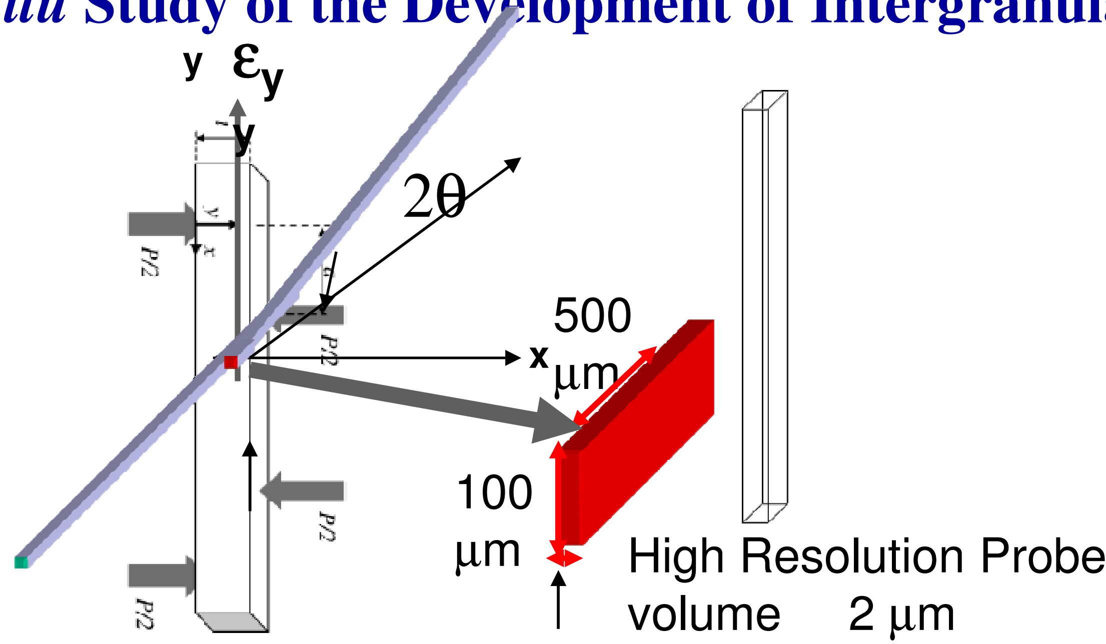

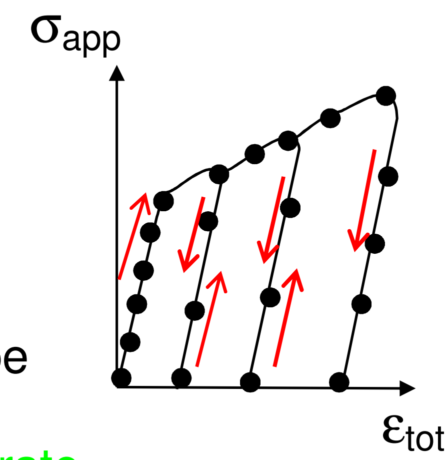

- Materials: Cementite/Ferrite; Ti-6Al-4V substrate
- New Alumina/Titania coatings with new bond coating
- New Titania (Rutile) coating, Amorphous Fe-C-B alloy coating
- Diamond Like Coatings, Aluminum alloy coatings,
- 4-point bending - unload cycle
- homogeneous plastic deformation macro/micro scopically
- Measured:
- Lattice strain response for individual phases and reflections.
- Total deformation by an in-situ 4-point bending

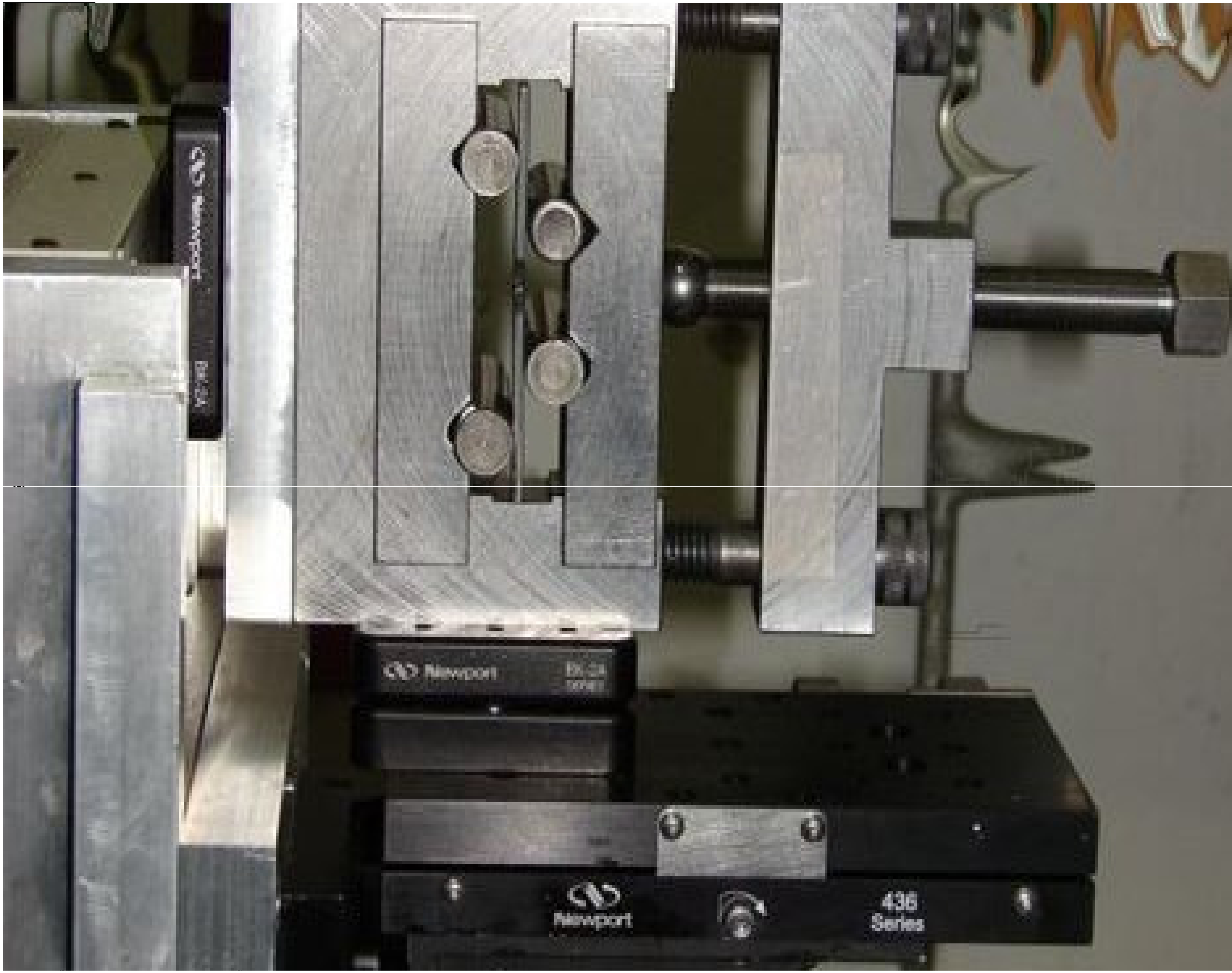
Newport
Newport
Newport
436
Series

4130 Steel

2 phases: cementite + ferrite

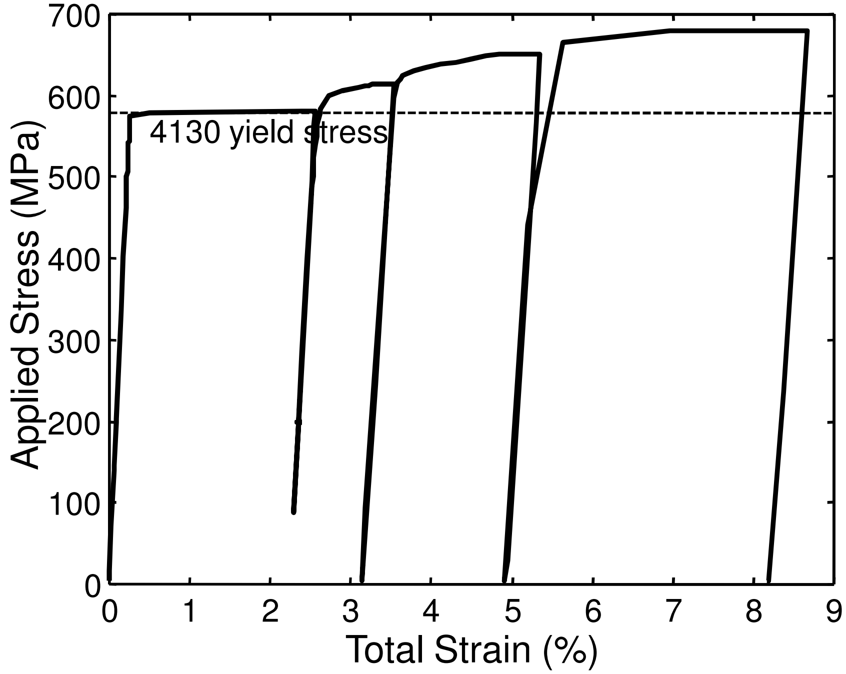

- Both 4130 steels subjected to 4-point bending loading
- Experiment carried out at BNL, NSLS source

  ⇒Rietveld Analysis

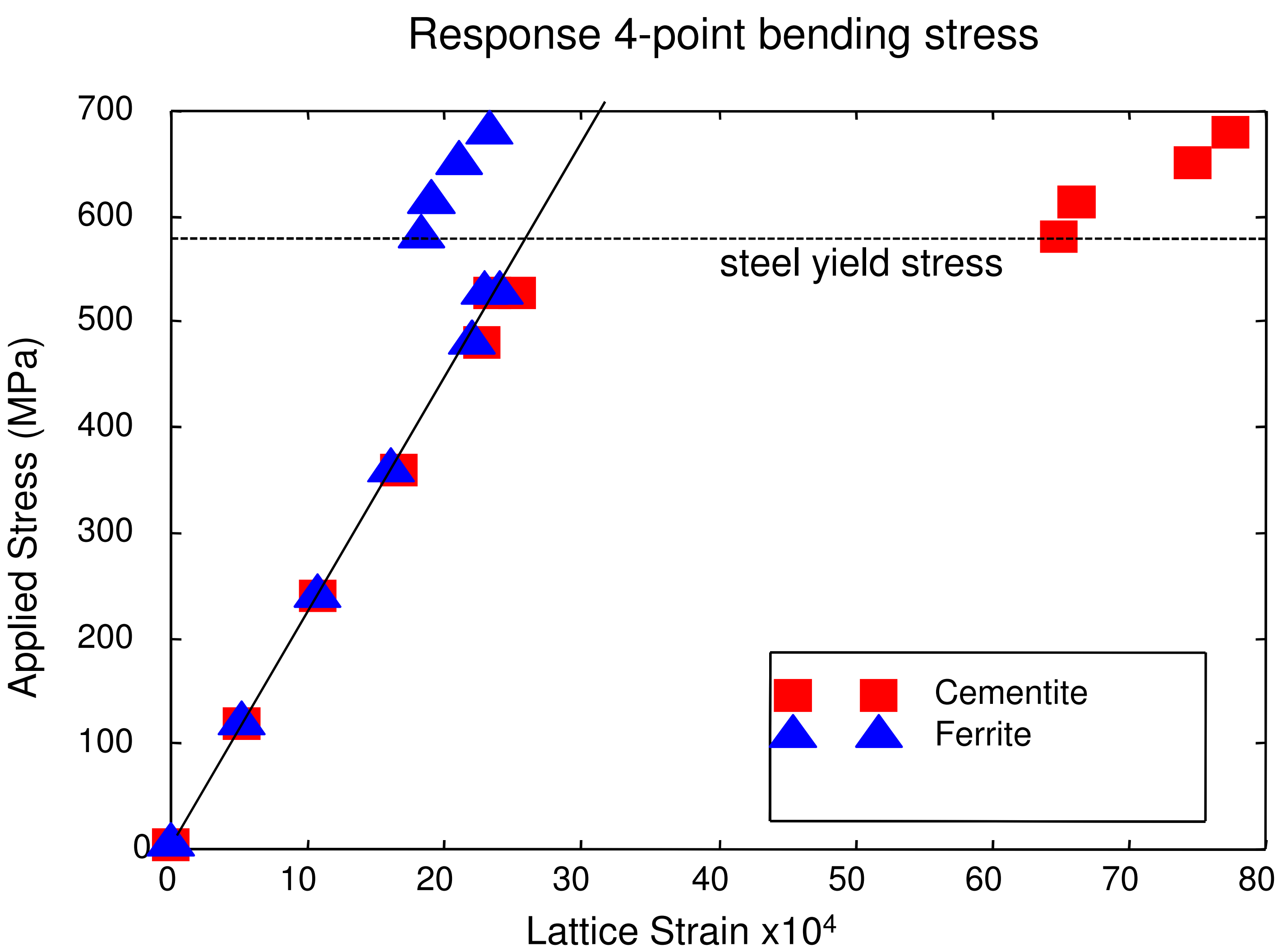
Response 4-point bending stress
Applied Stress (MPa)
700
600
500
400
300
200
100
0
0
10
20
30
40
50
60
70
80
Lattice Strain x10^4
steel yield stress
Cementite
Ferrite

NSMG

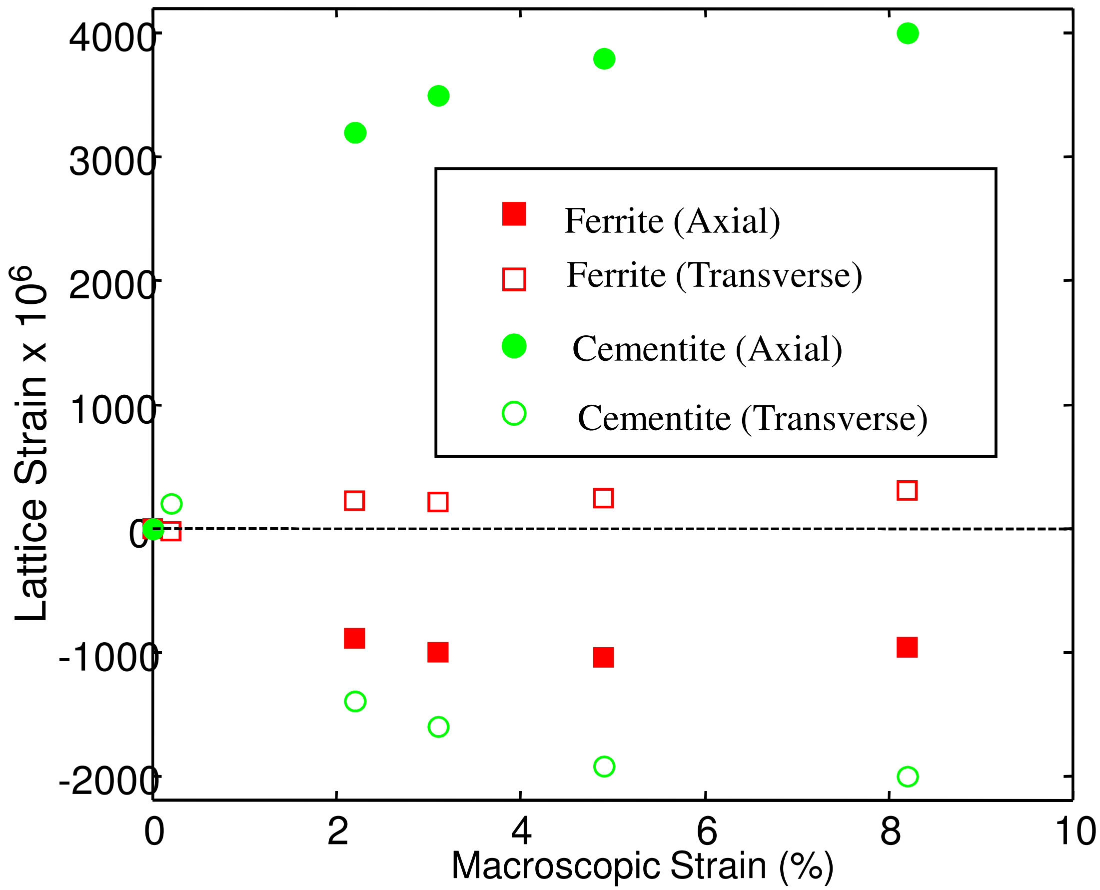

- σ_{33}/σ_{11} = -2 (Upper bound model)
- Vol. Fraction (Data) = 10 %
- Manufacturer specification = 9 %

Lattice strain response for Individual Reflections in steel

Response // x Axis

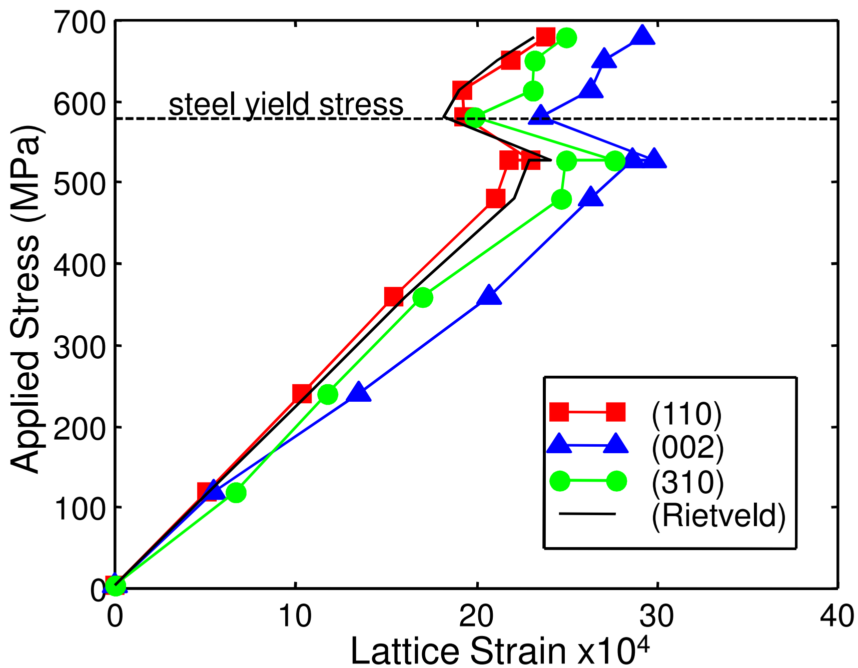

Response // y Axis

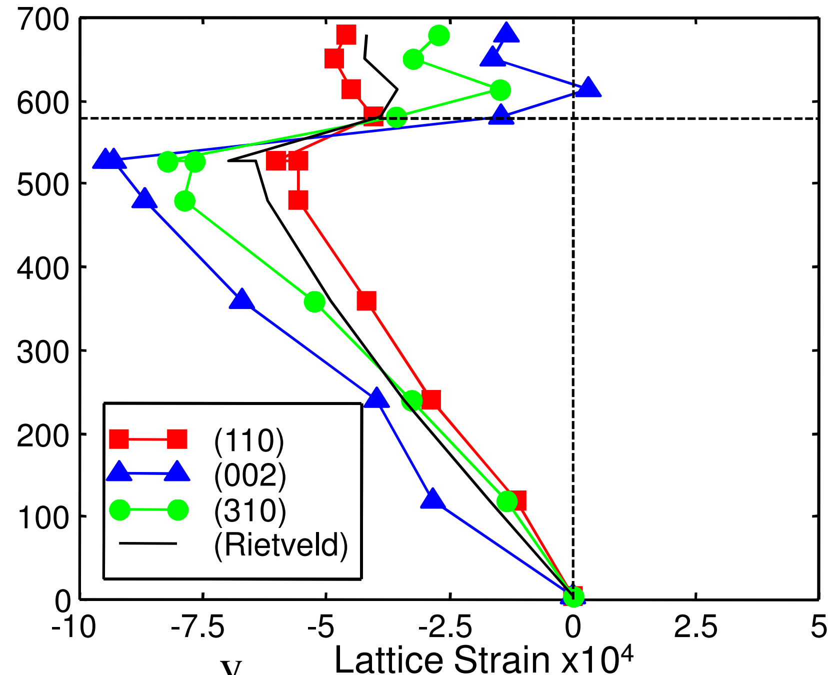

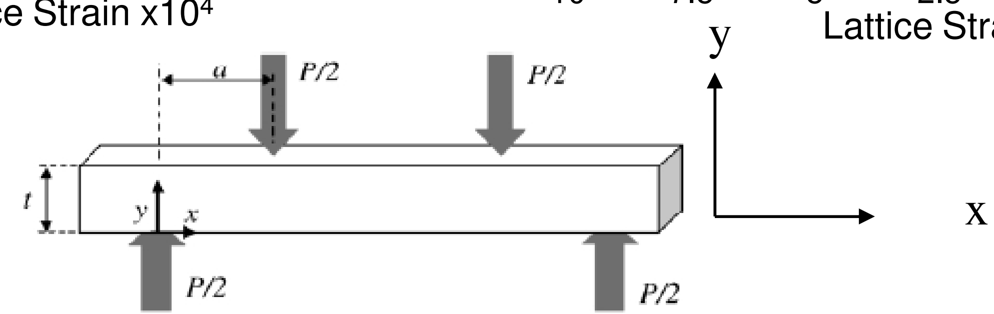

Ti-6Al-4V /Substrate

Thermal and Mechanical:

Ti-6-4:

- Young's Modulus = 115 GPa
- Poisson's Ratio = 0.349
- CTE = $10 \times 10^{-6}\ K^{-1}$

Distribution of α and β phase of Ti6Al-4V as a function of Temperature

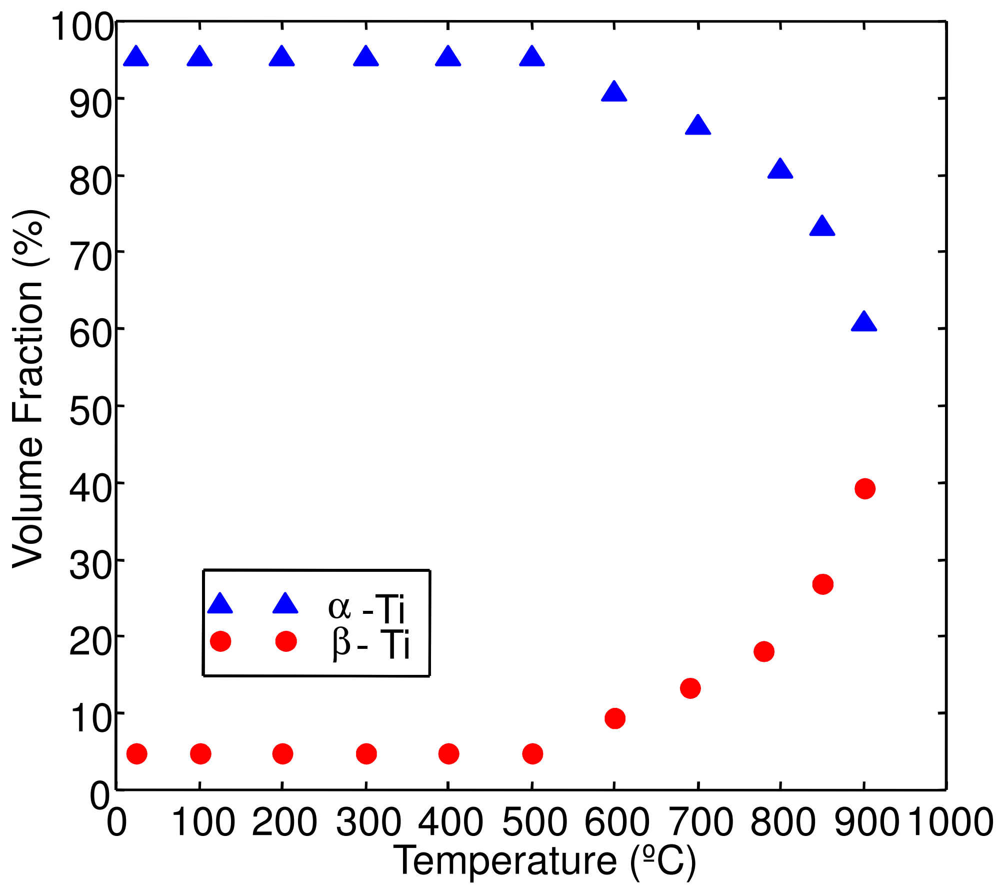

NSMG

Thermal strain in α and β phase of Ti6Al-4V as a function of Temperature

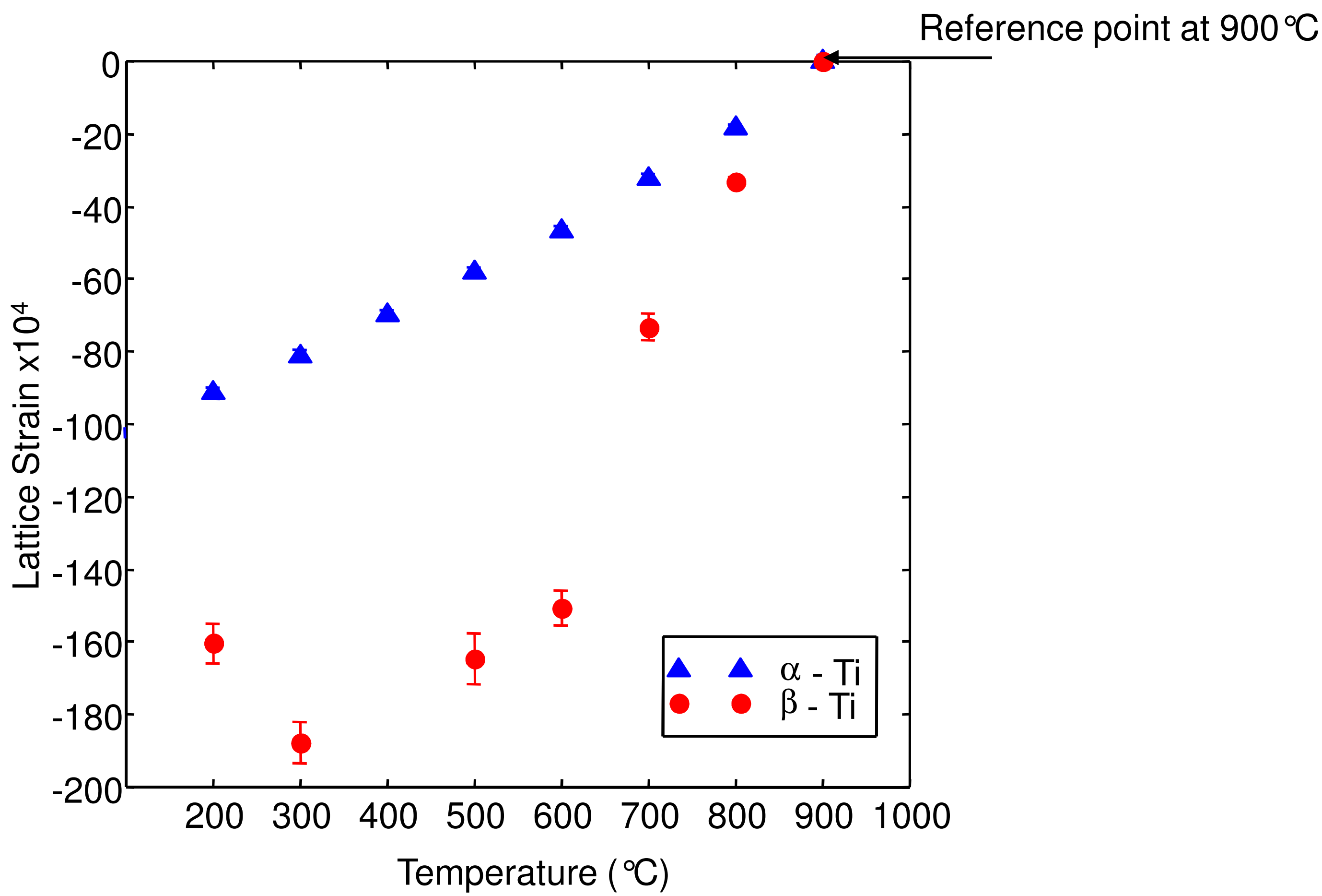

NSMG

Welcome to Rutgers
The State University of New Jersey

Thermal Sprayed Nanostructured Coatings

- *n*-Al_2O_3-13TiO_2 coatings fabricated by conventional plasma spray
- 2X the bond strength and 4X the wear resistance
- Extraordinary deformability without failure
- Direct transition to fleet and industry (fully commercial)

Patricia.Gruber

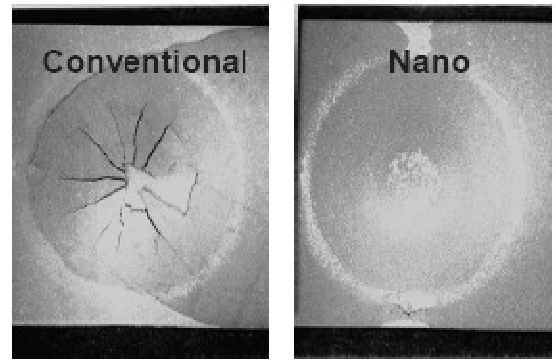

No failure even after
Severe deformation

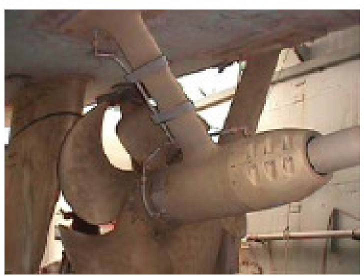

MCM shafts fail after 18months service
Requiring dry docking for weld repair

Uncoated shaft experiences
Severe scoring damage

No visible damage after
Four years of service

Courtesy Dr. Larry Kabacoff and Dr .Patricia Gruber ONR ISOPE 2007

Advanced Coating Technology Development for Enhanced Durability and Reduced Cost in Naval Applications

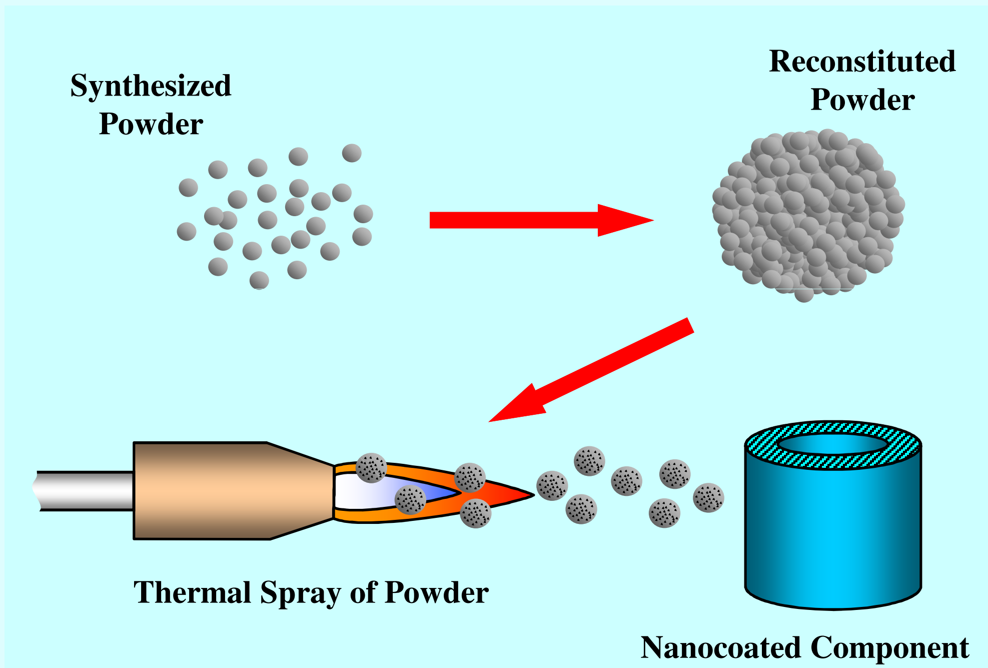

Courtesy Dr. L. Kabacoff ONR

Fundamentals of the Process

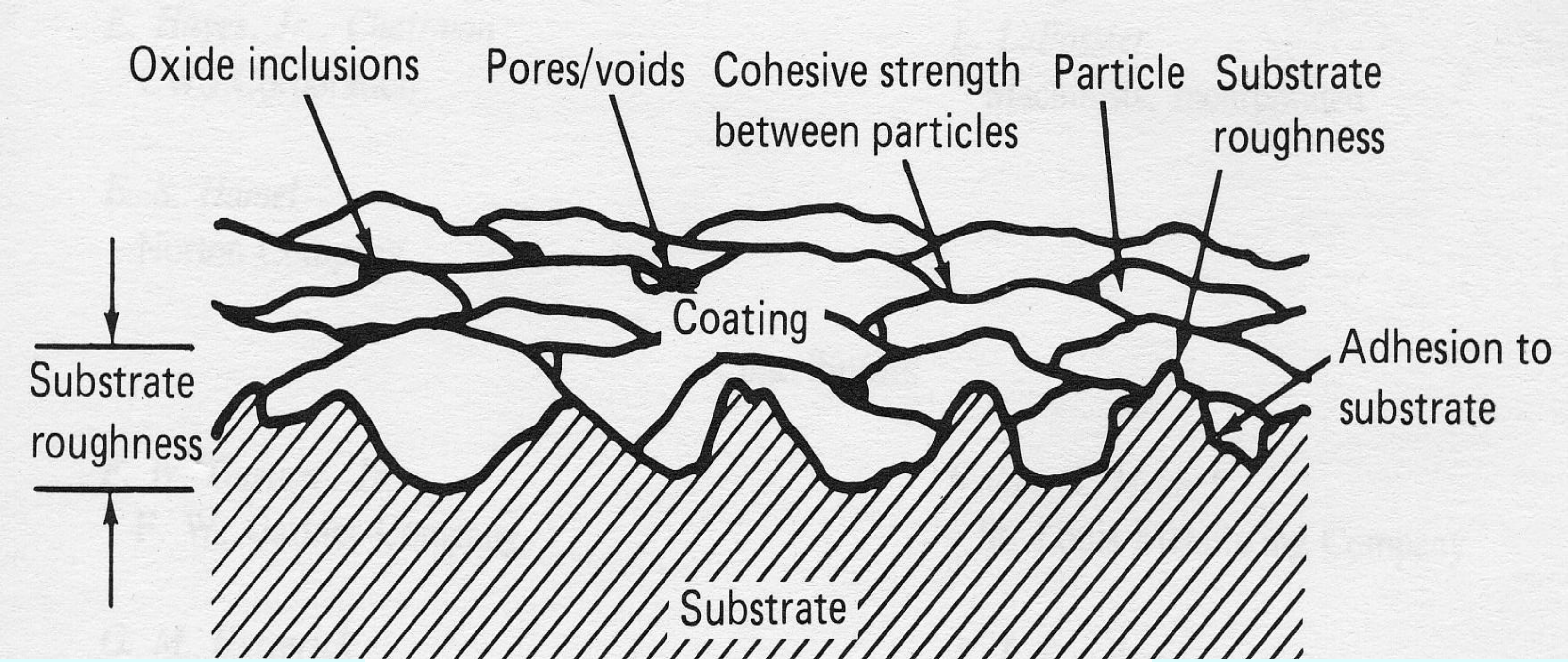

Coating Properties

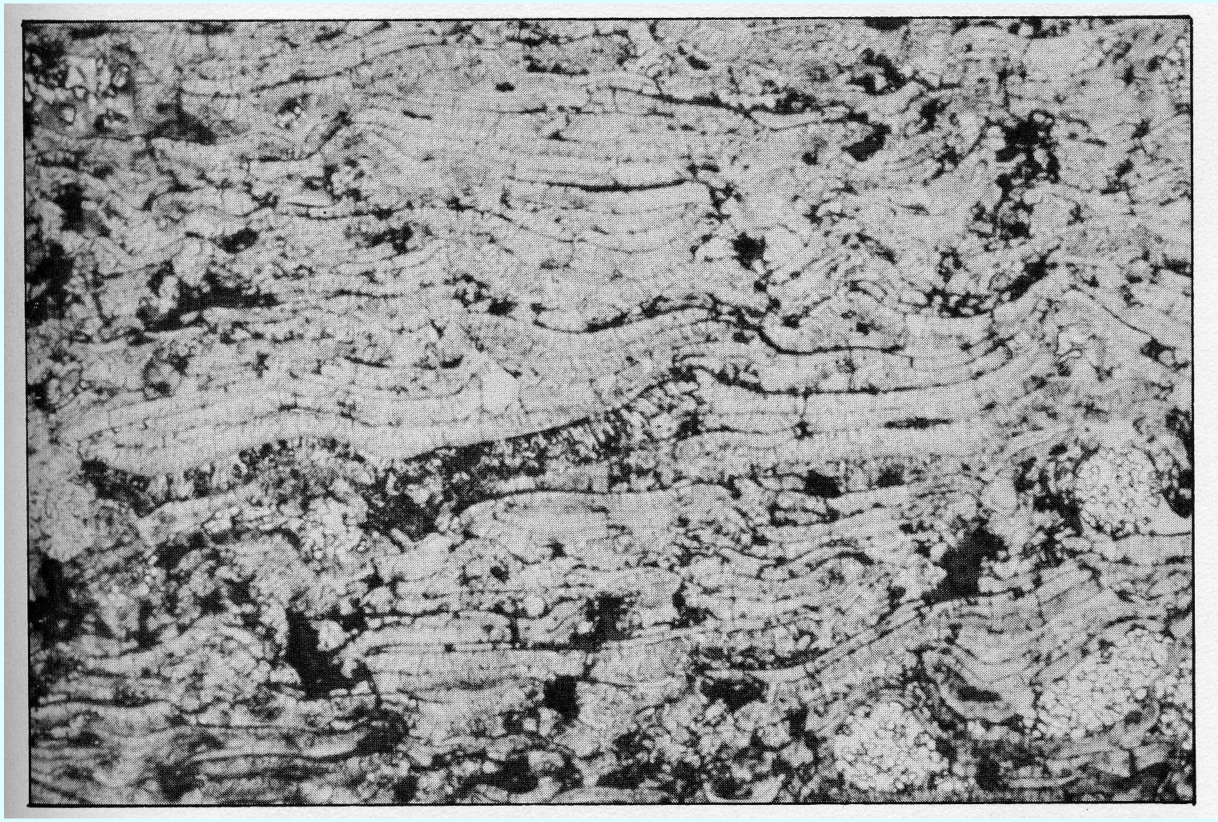

Material Systems

1. Al_2O_3-13wt%TiO_2 coatings made from starting micron size (Metco 130) and nanosized powders (Inframat 2613)(Particle size 20-30 nm) With Grit Blasting

In addition we compared the phases and strains as a function of coating thickness in both micro- and nano- coatings.

Substrates: 1) 1020 Steel (with a Ni bond coat)

2) Titanium (with a Ti bond coat)

Varying thickness of micro- and nano- coatings were applied.

Substrates were grit blasted (compressive stresses).

Table 1, summarizes the coating samples produced with 1020 steel. Table 2 is similar for the titanium substrate coating samples produced.

All the samples were prepared by A&A company,

Ti substrate samples

Starting Powder	Substrate	Coating thickness	Designation
Micron	Titanium	None	T1
		Grit blast only	T2
		Grit blast and bond coat	T3
		2 passes on T3	T4
		Typical coating on T3	T5
		Over-coating, on T3, before failure	T6
		Over-coating, on T3, after failure	T7
Nanosize	Titanium	2 passes on T3	T8
		Typical coating on T3	T9
		Over-coating, on T3, before failure	T10
		Over-coating, on T3, after failure	T11

Phase Mapping

A series of EDXRD spectra as a function of (x_3) depth for a nano-alumina-titania coating on a Ti substrate. Note that the spectra are displaced equally so that the coding region can be seen. The Miller indices for the Ti (hcp) substrate and the spinel structure phase in the coating are indicated.

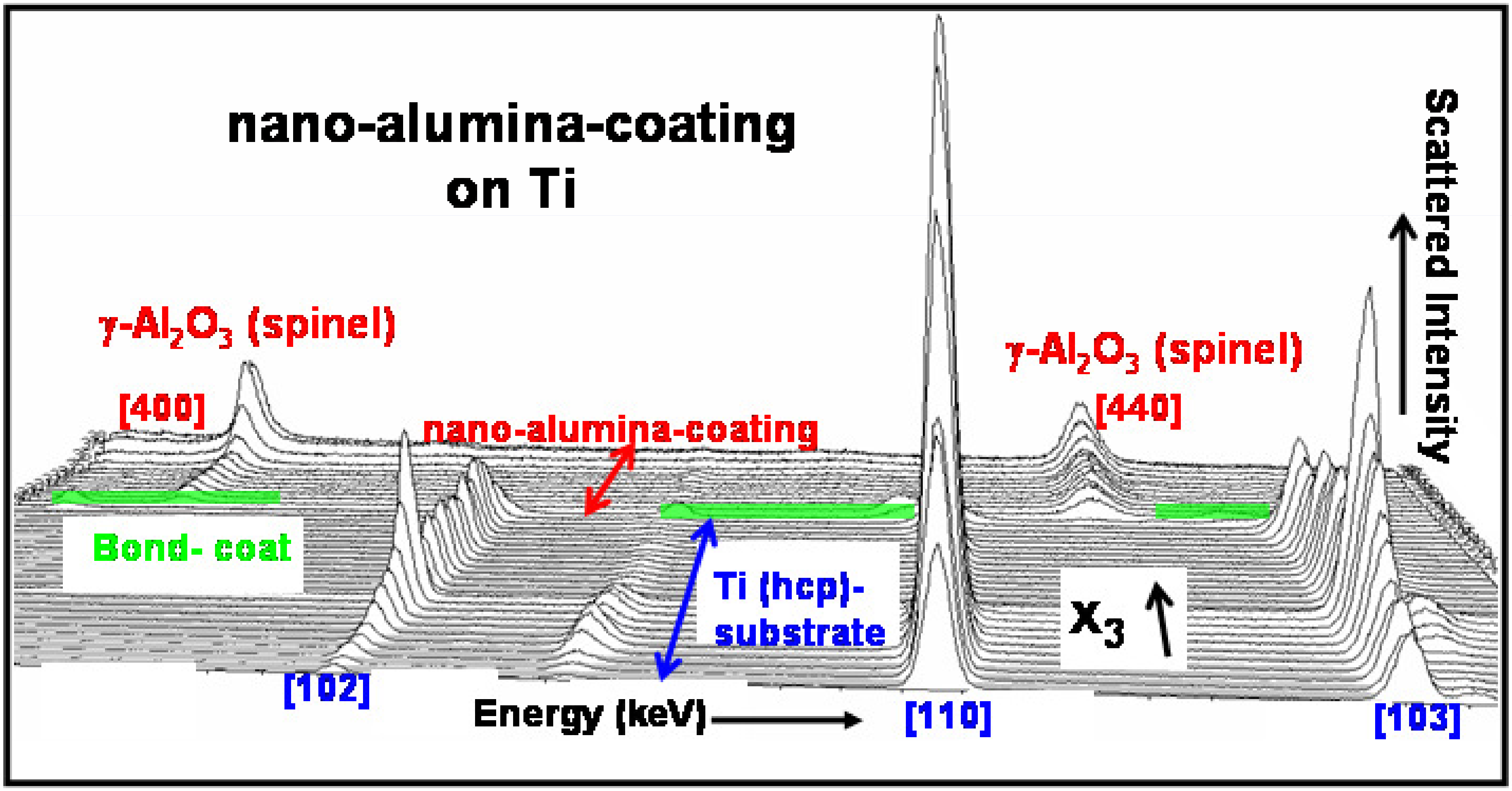

Phase Mapping

Wide view of EDXRD patterns of powders obtained by delaminating TS titania-alumina coatings under 4-point compression and then grinding the coating into powder. The T5 is a typical thickness micro-coating and T9 is a typical thickness nano-coating. Note: the γ-Al_2O_3 spinel and α-Al_2O_3 corundum Bragg line indexing; the expected Ce atomic fluorescence lines in the nano material; .

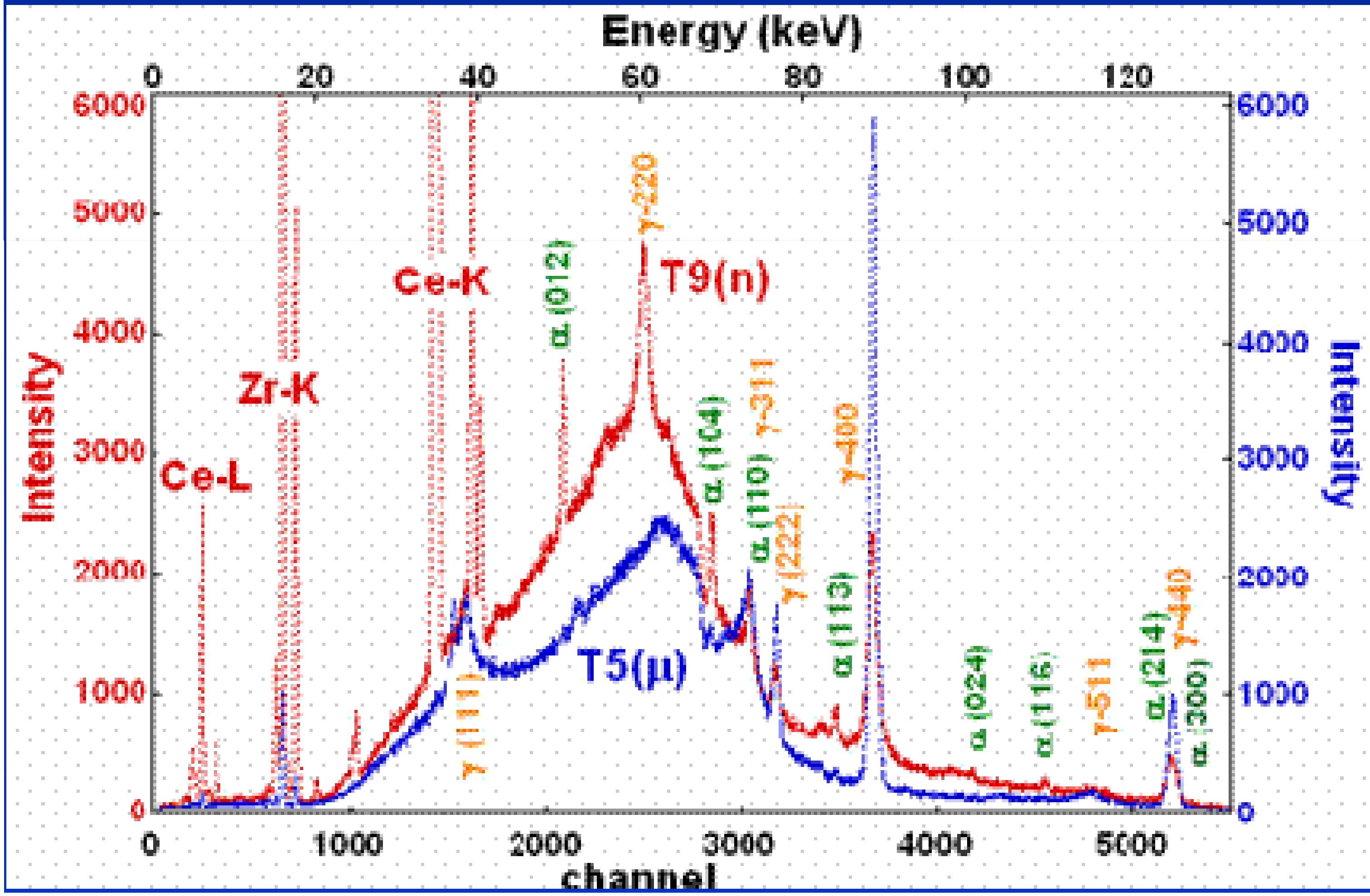

Phase Mapping

The γ-Al_2O_3 spinel γ-400 Bragg line for the T5(micro)- and T9(nano)-coating powders. This is the line used to evaluate the strain variations in the coatings. Note: the strong broadening of the small grain size nano material line relative to the micro material; the nano- material is dilatation of the lattice parameter by +0.2% relative to the micro-material; the prominent α-Al_2O_3 corundum phase Bragg line in the amorphous phase.

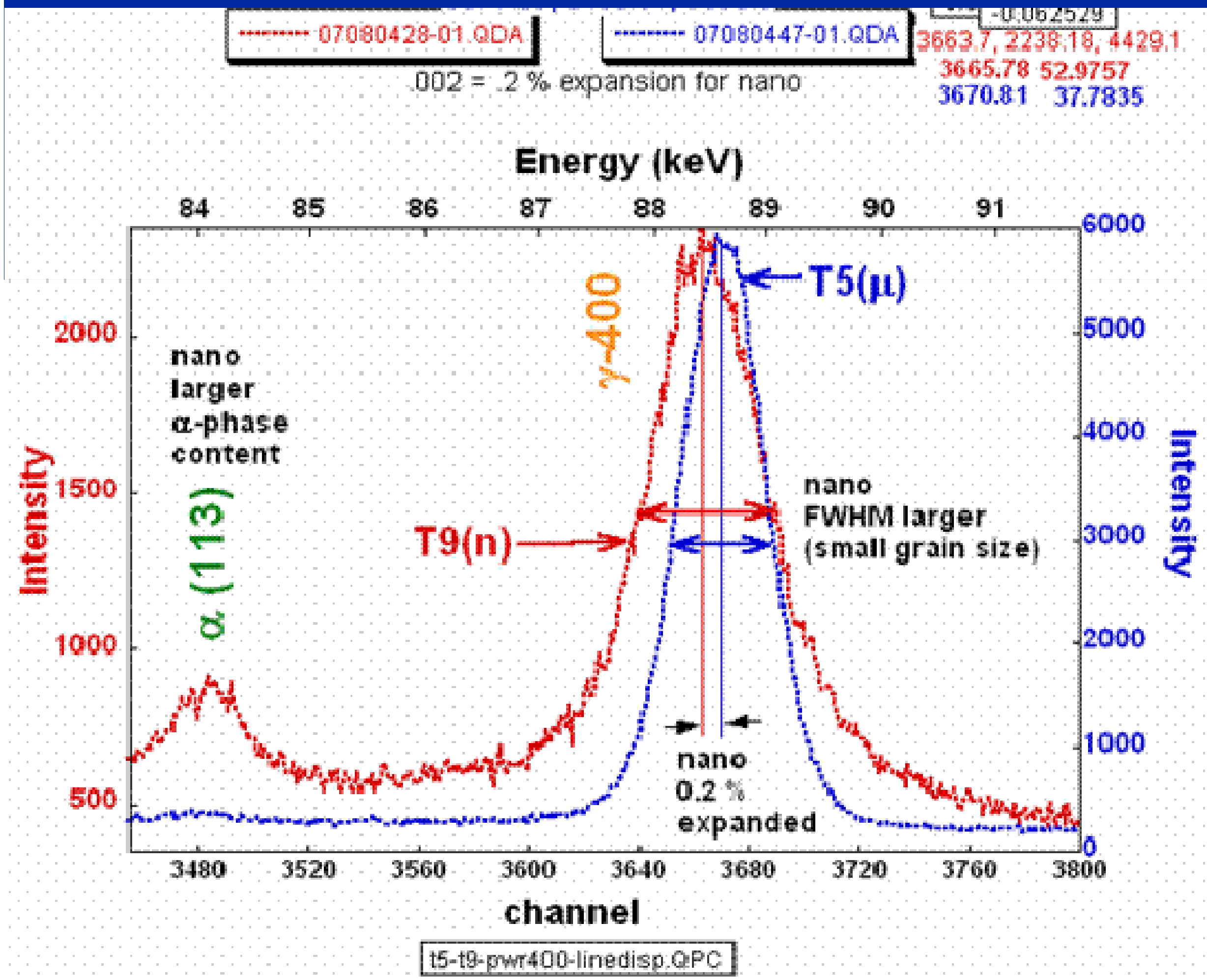

Phase Mapping

Ti-K edge XAS near edge structures for a series of Ti compounds. The pre-edge features are shown on an expanded scale in the inset of the figure. Comparison of the n- and µ-feed powder spectra are to the anatase phase TiO2 standard clearly confirm this as the the feed powder phase in both cases. The Ti environment in the plasma sprayed (PS) n- and µ- coatings are dramatically differend and are unambiguously not anatase phase. Note that the FS oscillations above the edge are sharper for the µ-PS-coating (relative to the µ-PS-coating). The broadening of the µ-PS-coating FS features are typical of a more disordered local environment as expected for nano-phase materials.

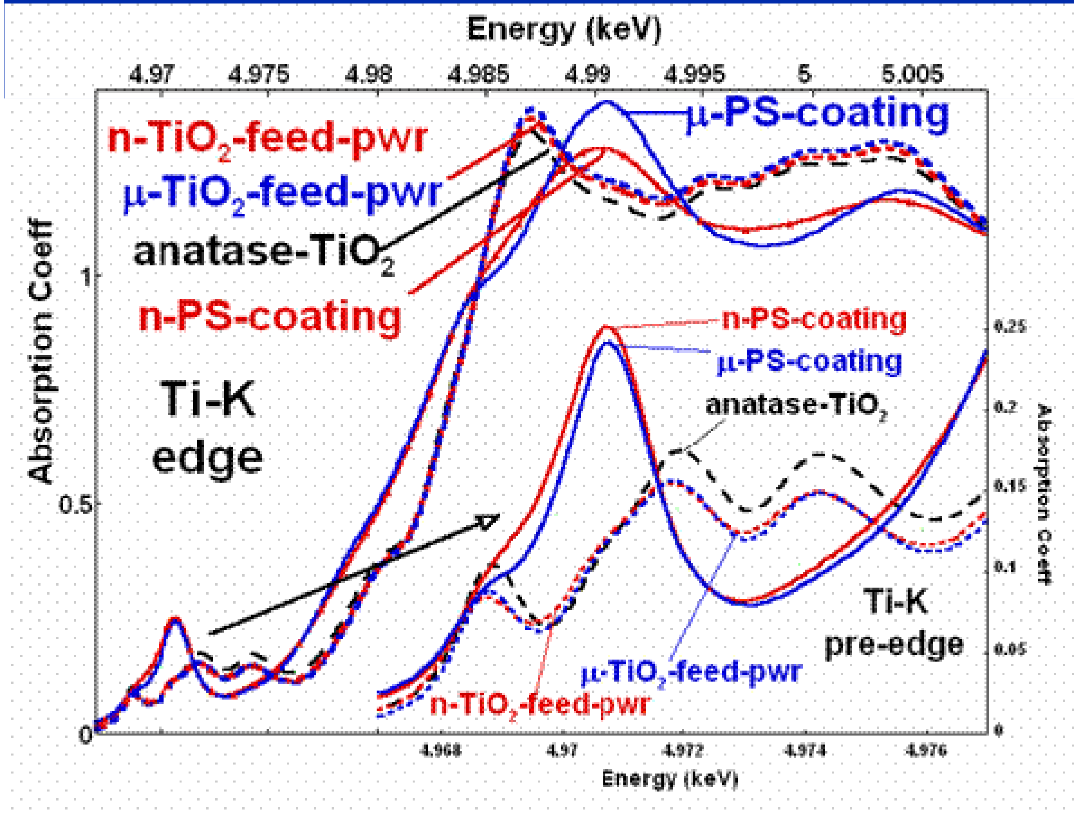

TiO_x , 2>x>1.5

Chemically reduced Ti.

Strain Mapping

A comparison plot of the ε_{33} strain in as-received titanium substrate, and grit blasted titanium substrate. It can be noted that in the grit balsted sample surface compression introduces a bending moment in the other underlying bulk material which is clearly visible by the sloping data between 0<x3<1.5

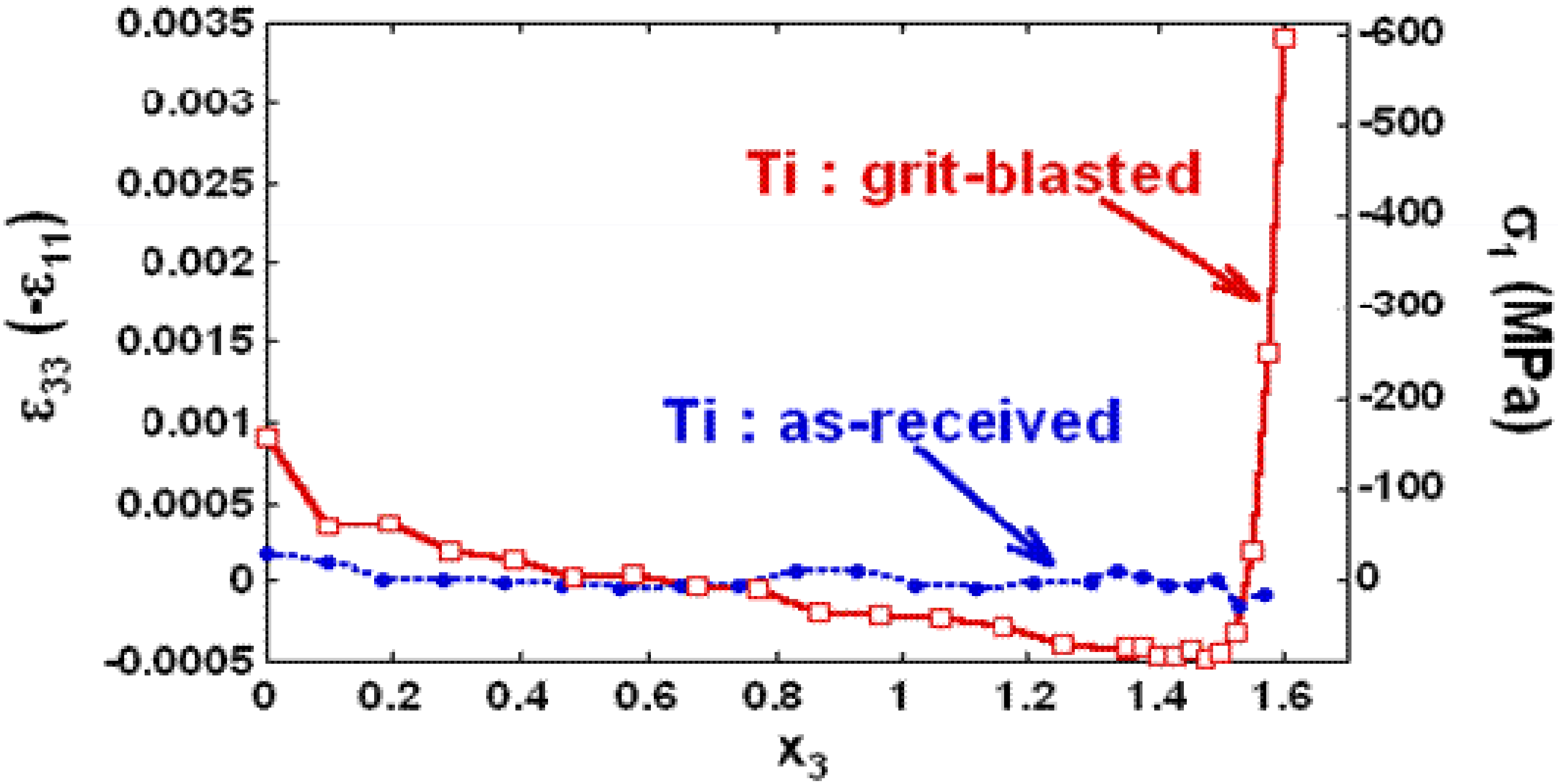

Strain Mapping

Effect of bond coat on compressive strain ε_{33} of Grit Blasted Ti

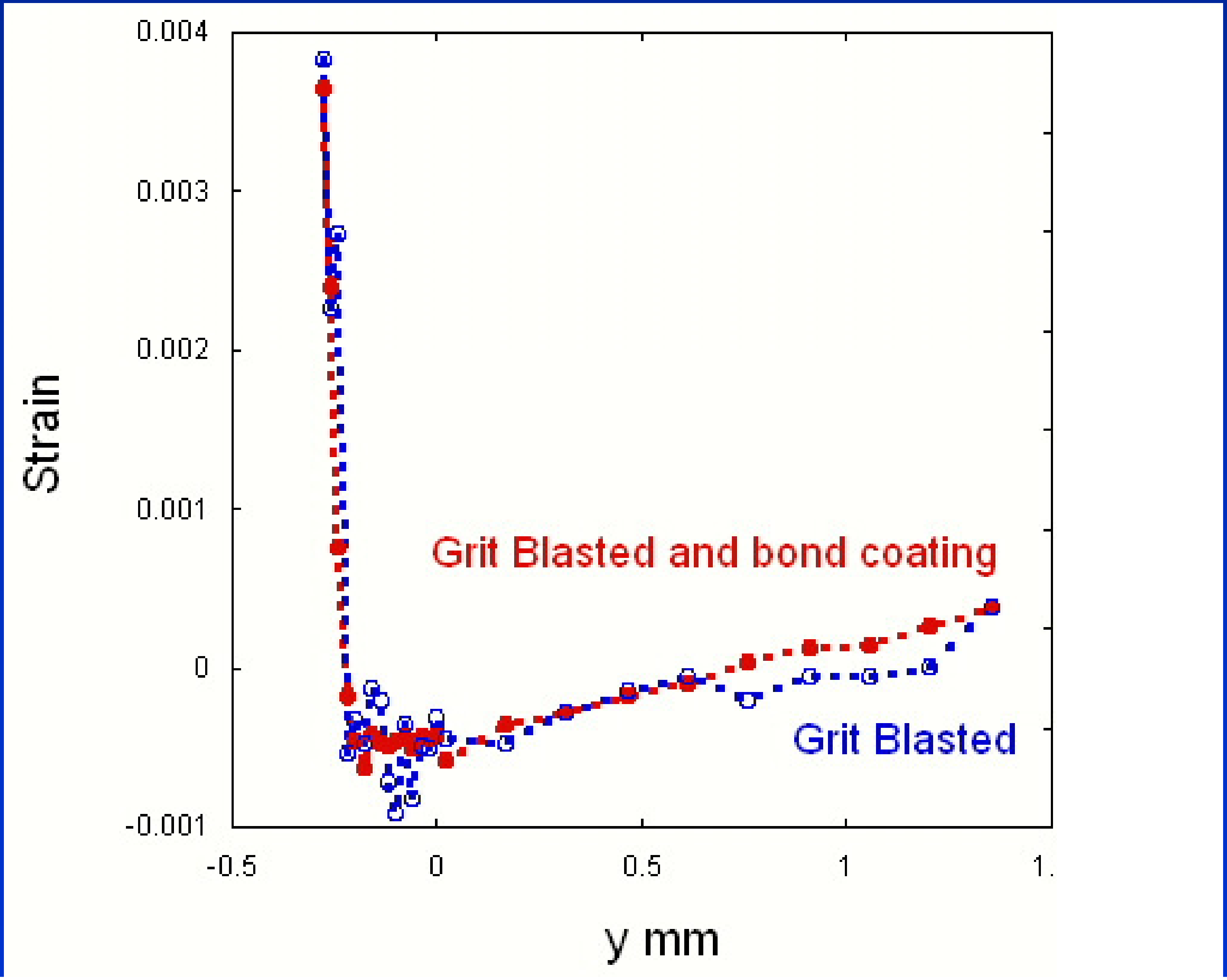

VALIDATION 2. <u>Grit Blasted</u>

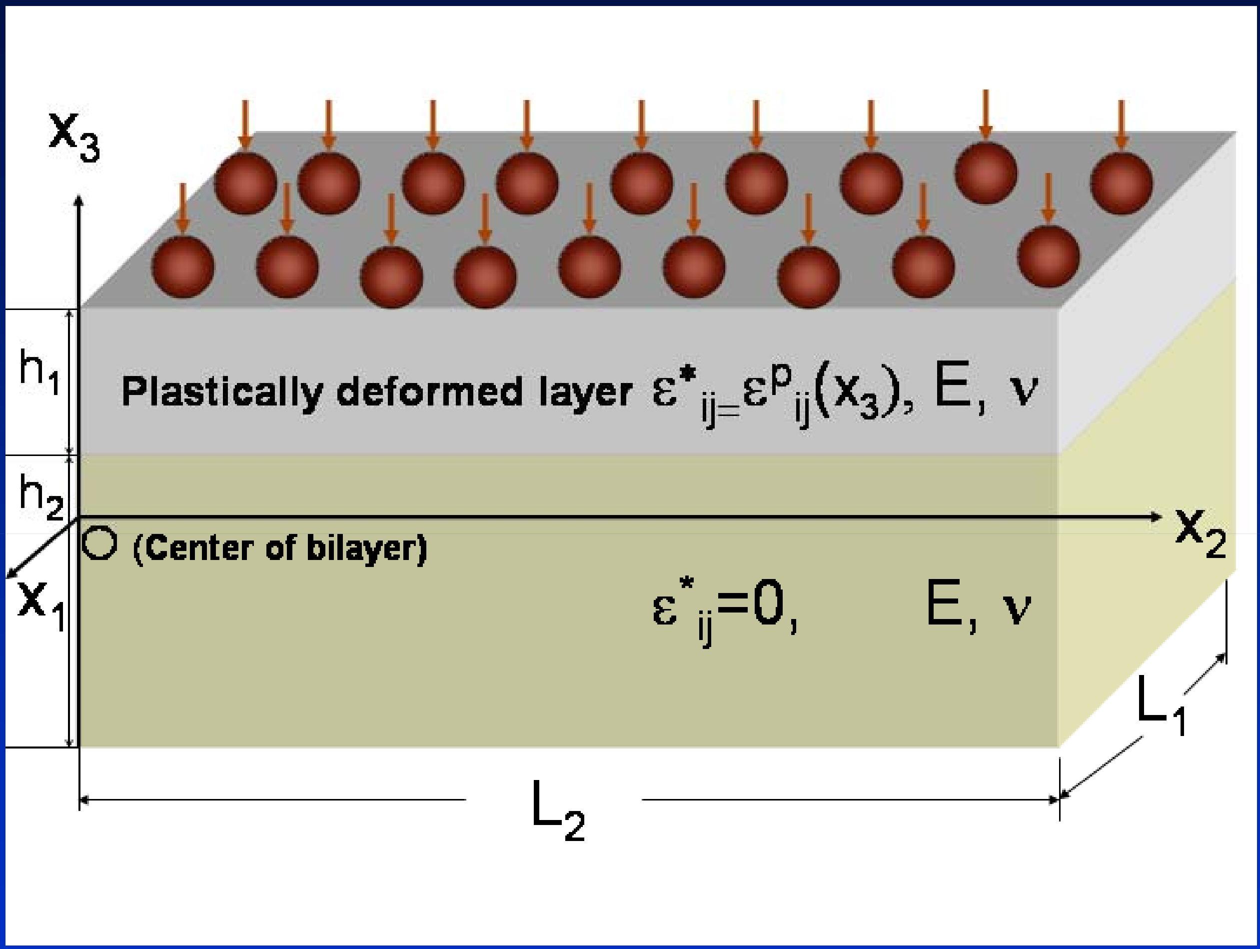

Schematic of model for Grit Blasted strains/stresses

EDXRD Grit Blasted; Steep strain gradients; High Resolution

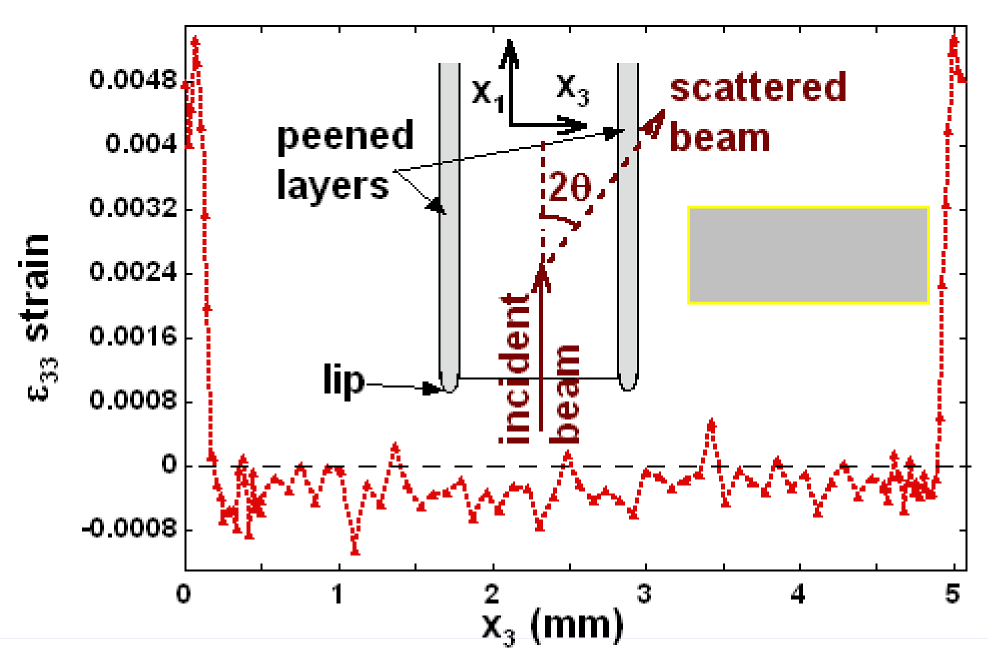

Strain profile of ε_{33} across the entire thickness of a Ti double-sided shot peened specimen. The inset shows schematic of the x-ray scattering geometry along with the definition of the coordinate directions. Note the schematic representation of the lip which was optically profiled in Figure above.

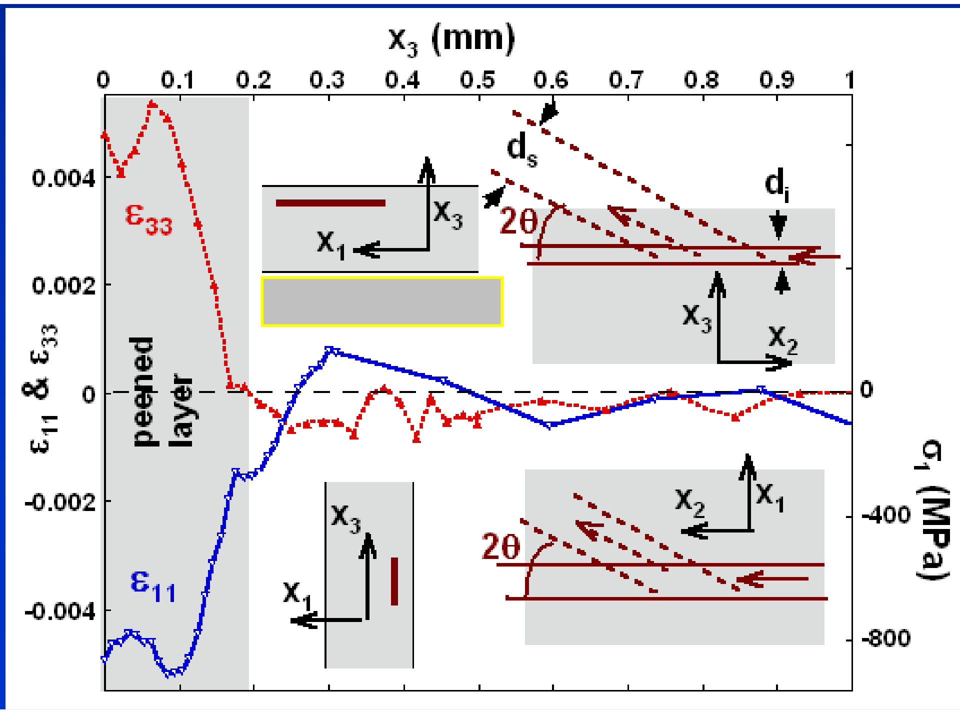

VALIDATION 2.

The strain profiles of ε_{33} and ε_{11} in the vicinity of the peened surface layer and the underlying bulk material of the Ti specimen. The insets illustrate the x-ray scattering geometries for the ε_{33} (top) and ε_{11} (bottom) measurements. Note the stress scale (lower right) uses E=118 GPa and ν=0.33 . **ε_{33} = - 2 ν/(1- ν) ~ - ε_{11}**

In-situ 4-point bending experiment Ti

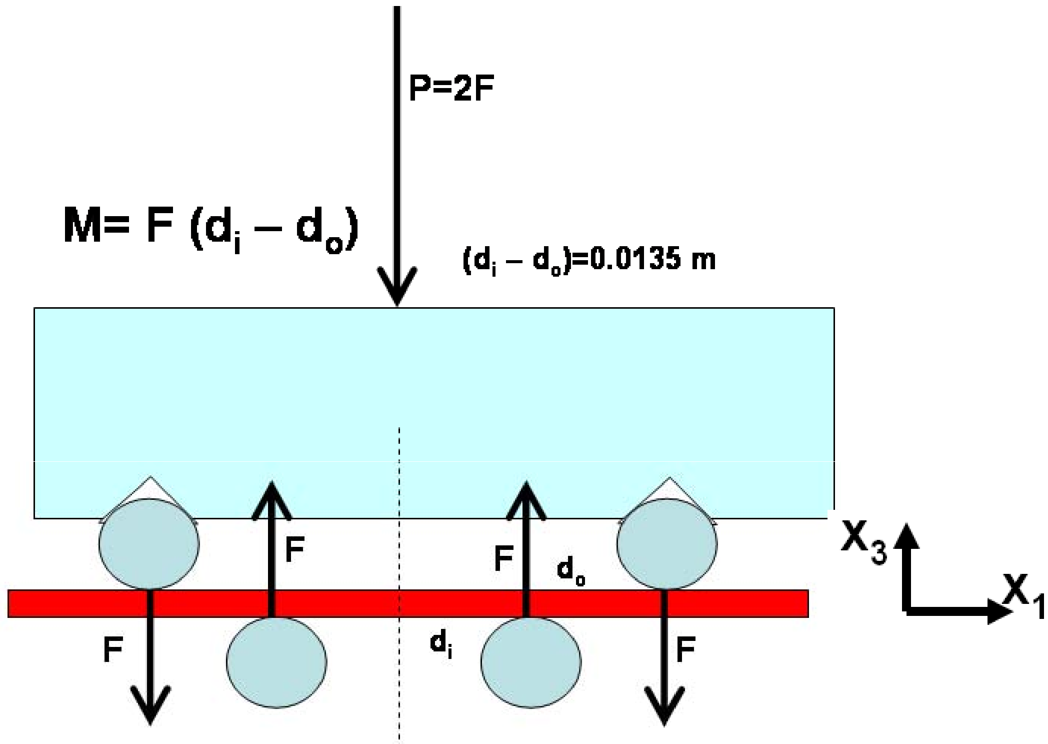

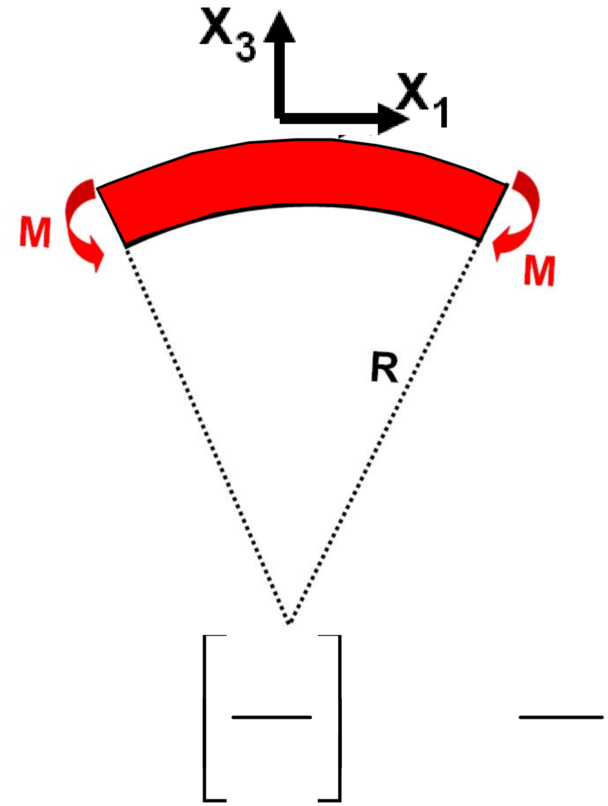

Linear depth variation

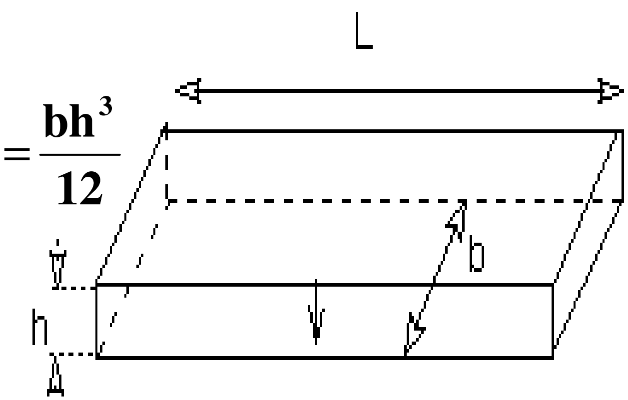

$$I = \frac{bh^3}{12}$$

Bending released: Residual stresses and bending

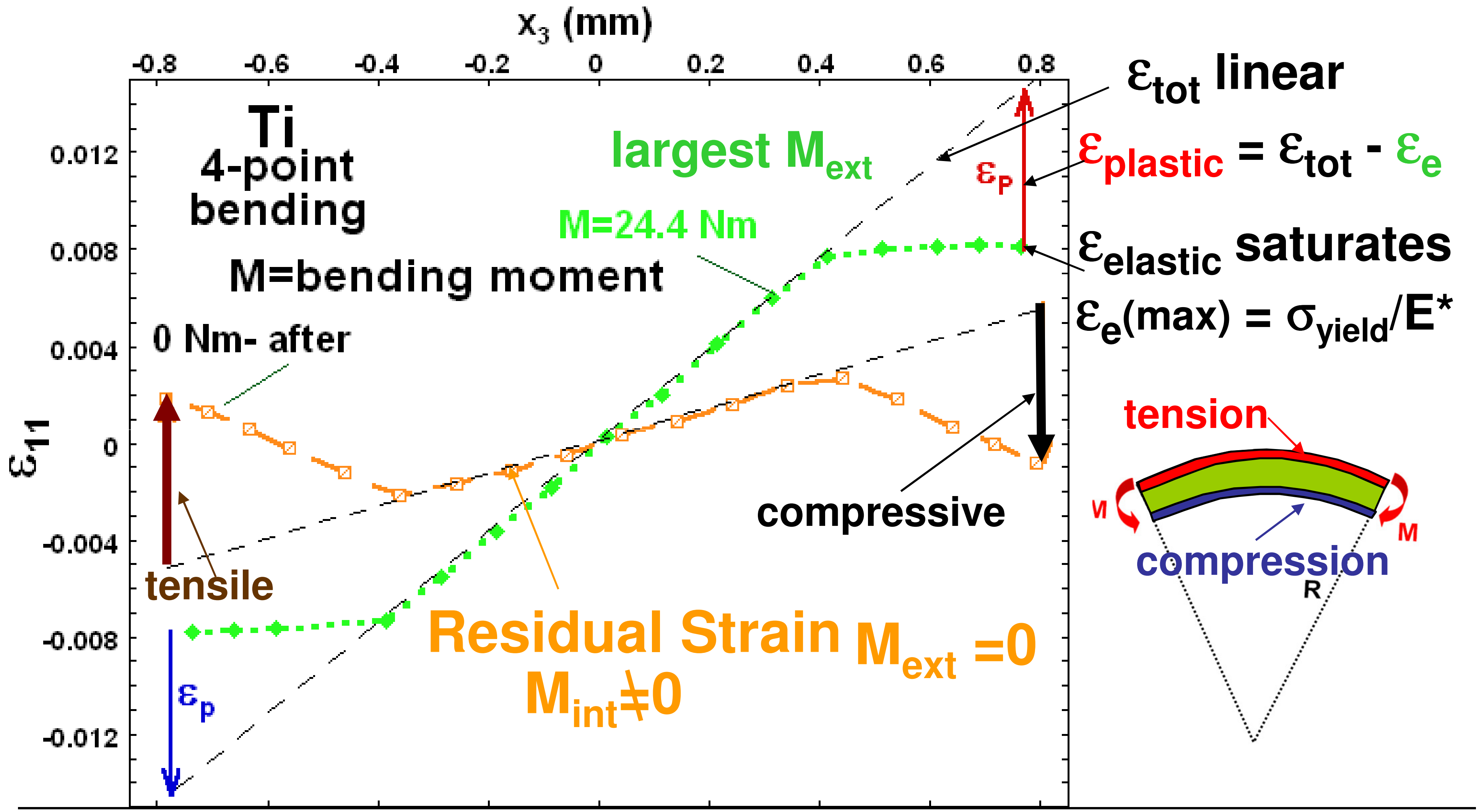

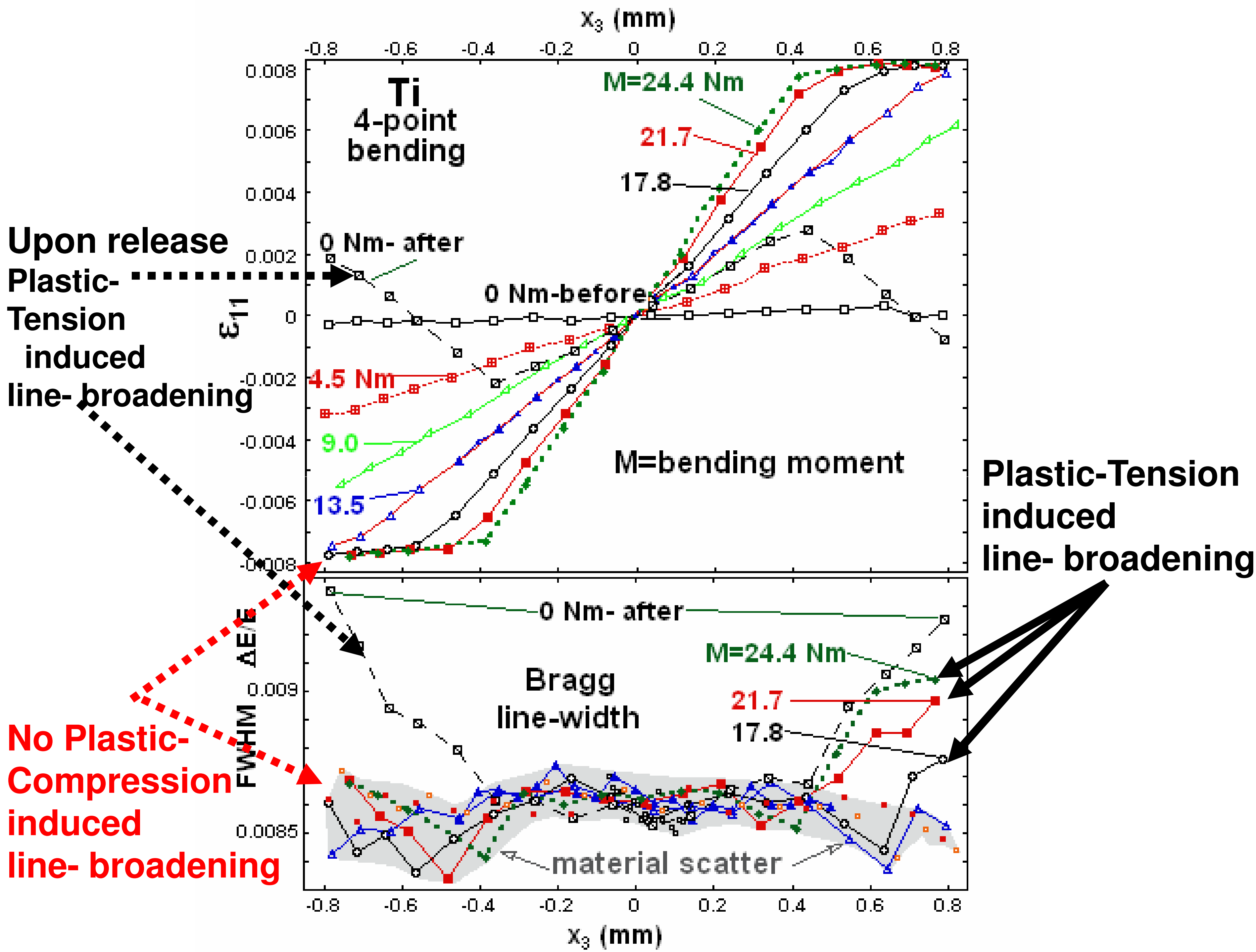

x3 (mm)
Ti
4-point
bending
M=24.4 Nm
21.7
17.8
0 Nm- after
0 Nm-before
4.5 Nm
9.0
13.5
M=bending moment
ε11
Upon release
Plastic-
Tension
induced
line- broadening
Plastic-Tension
induced
line- broadening
No Plastic-
Compression
induced
line- broadening
FWHM ΔE/E
0 Nm- after
M=24.4 Nm
21.7
17.8
Bragg
line-width
material scatter
x3 (mm)

Modeling and Theory

Four-point Bending of substrate and coatings plates

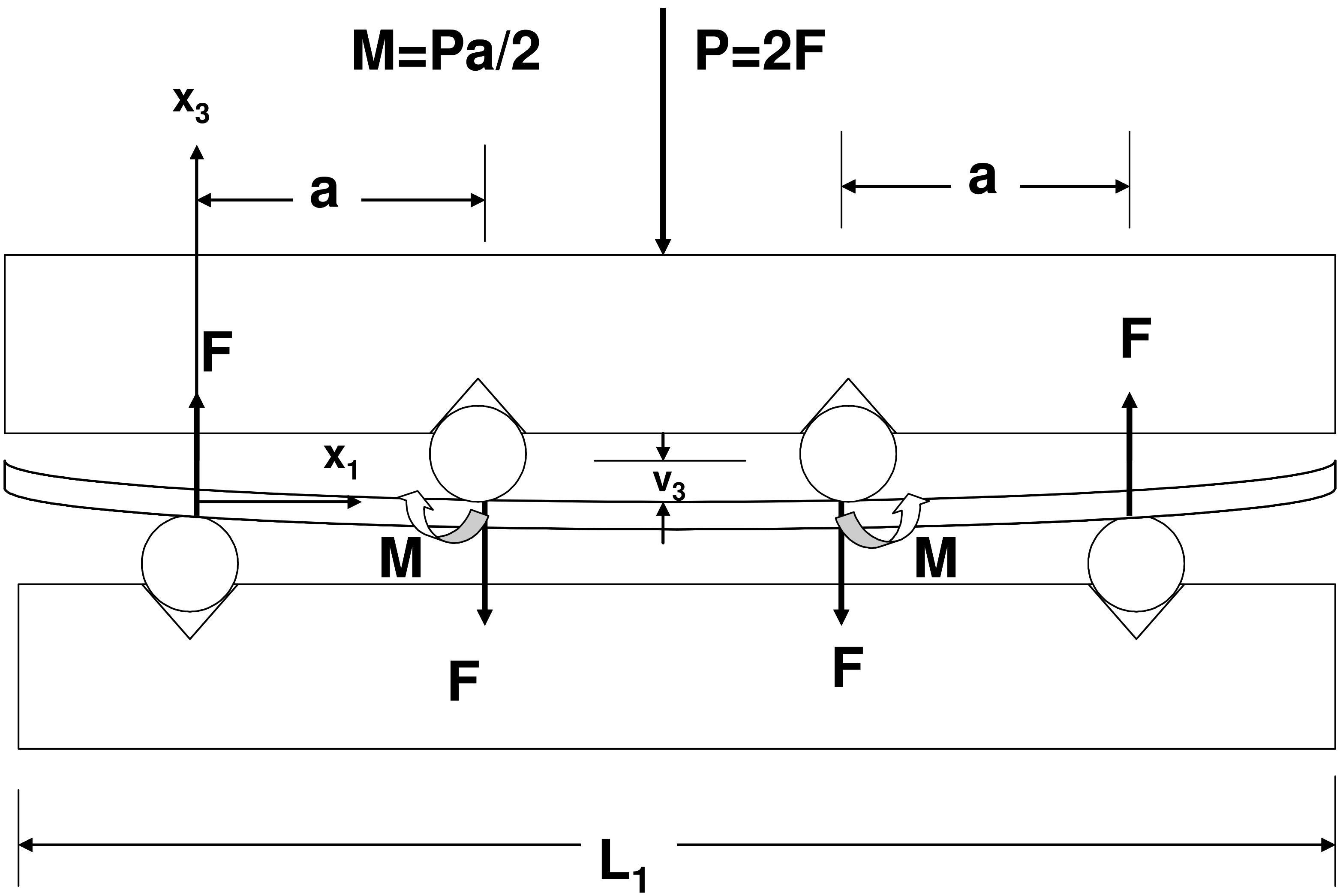

Strain Mapping

ε_{11} depth (x_3) variation profiles of of DLC/4142 steel substrate test specimen at various load levels in the four point bending geometry

Phase Mapping

ε_{33} depth (x_3) variation profiles of of alumina-titania-coating/Ti-substrate test specimen at various load levels in the four point bending geometry.

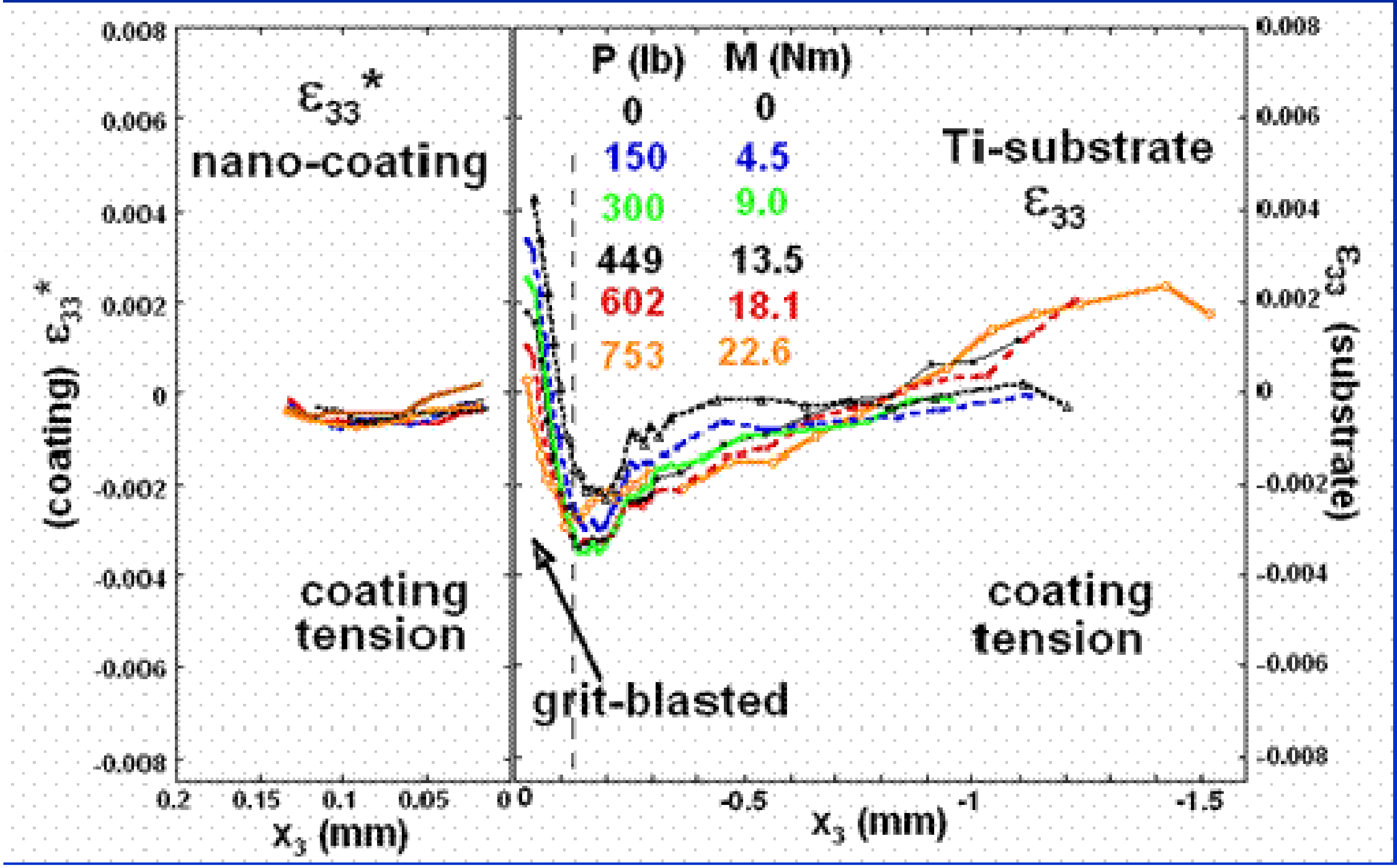

Eigenstrain Modeling

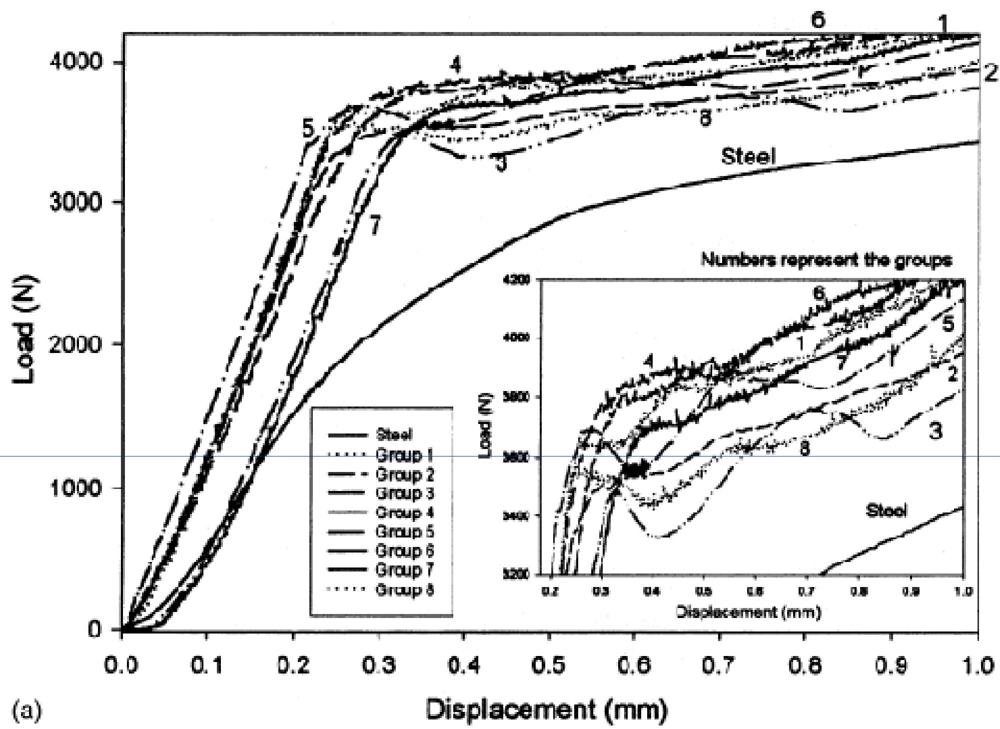

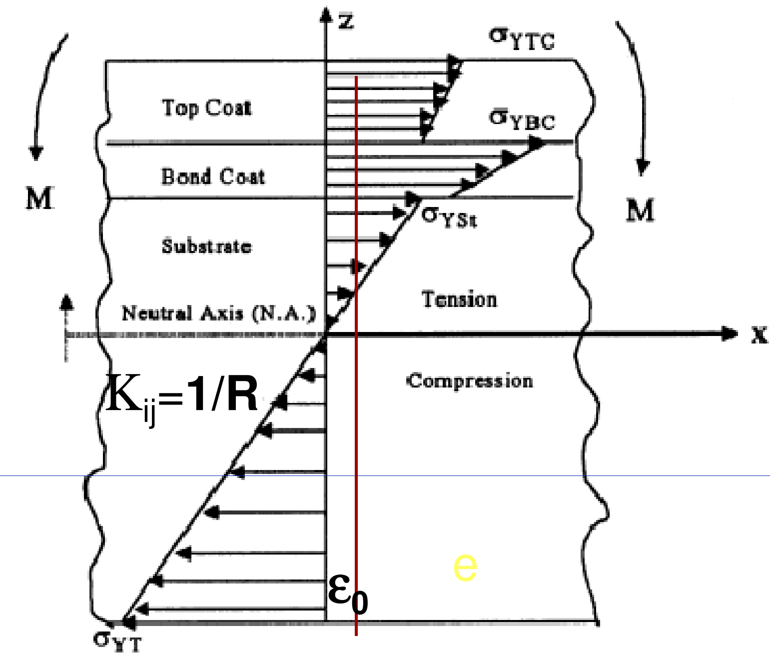

Fig. 2. Schematic illustration of the bending stress in the coating under four point bend test.

Eigenstrain Analysis

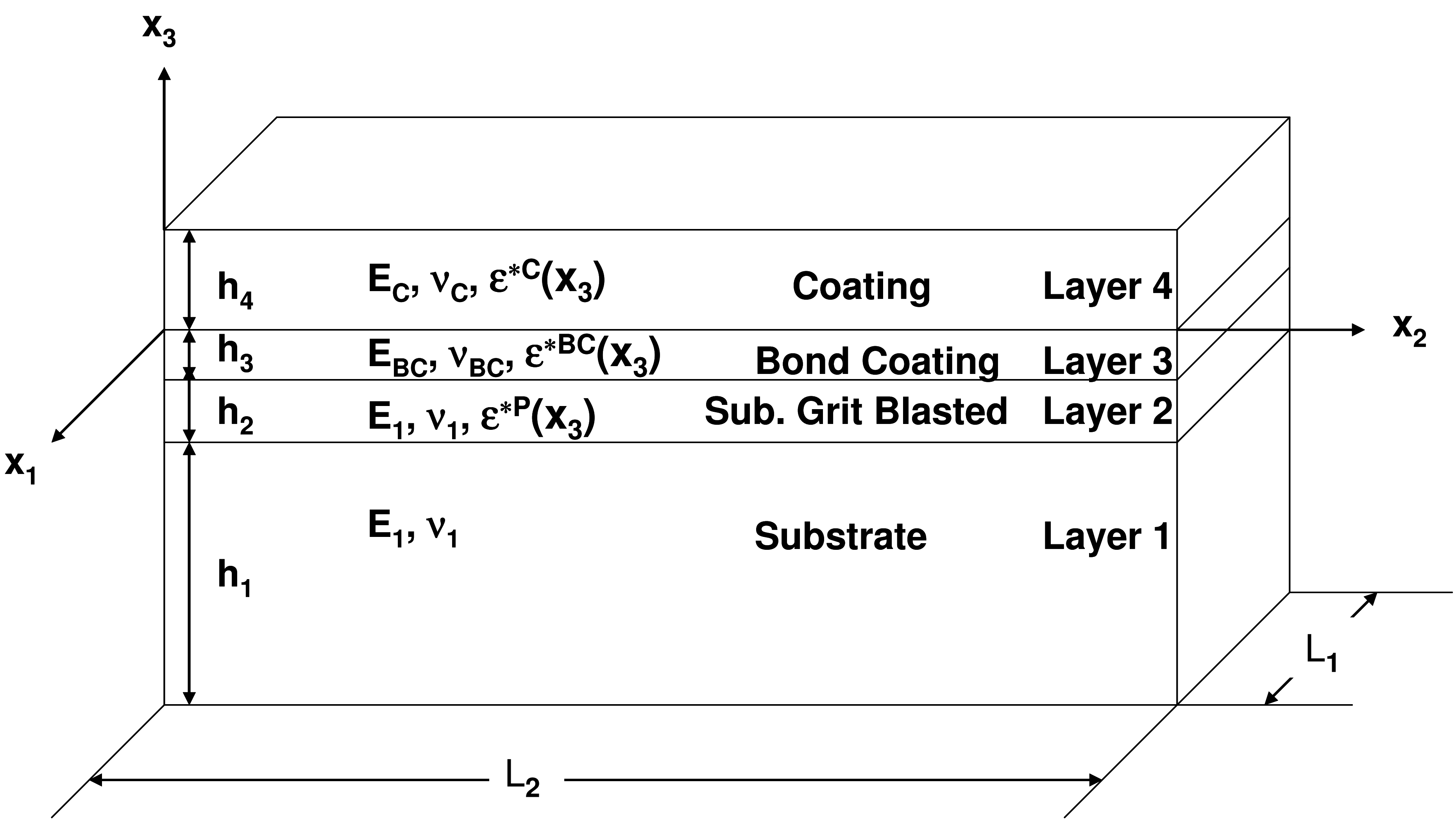

Schematic of the layered stack structure of the substrate/coating materials systems used in this study

stresses and strain –the elasto-plastic analysis Eigenstrain

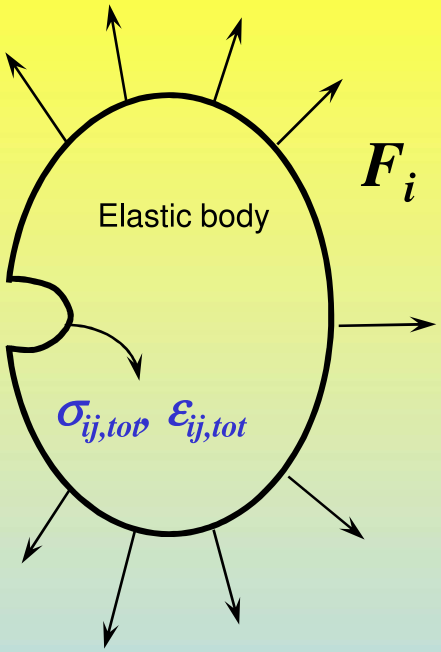

Multiaxial stress state

$$\begin{cases} \sigma^{e}_{ij,net}\varepsilon^{e}_{ij,net} = \sigma^{a}_{ij,tot}\varepsilon^{a}_{ij,tot} \\ \varepsilon^{a}_{ij,tot} = f\left(\sigma^{a}_{ij,tot}\right) \end{cases}$$

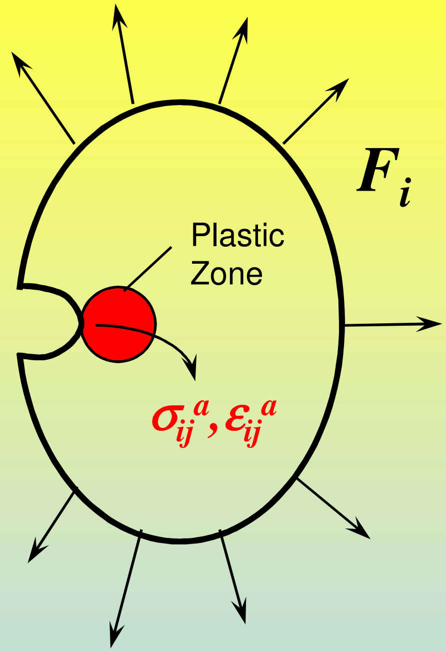

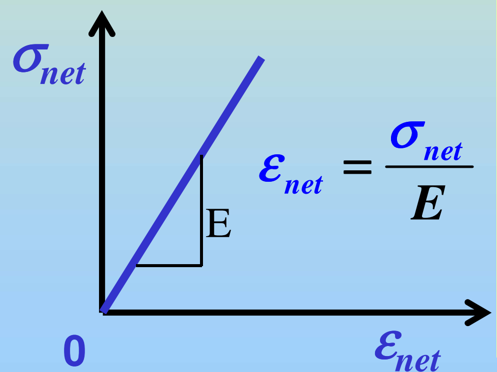

Uniaxial stress state

$$\begin{cases} \sigma^{e}_{22,net}\varepsilon^{e}_{22,net} = \sigma^{a}_{22,tot}\varepsilon^{a}_{22,tot} \\ \varepsilon^{a}_{22,tot} = \frac{\sigma^{a}_{22,tot}}{E} + \left(\frac{\sigma^{a}_{22,tot}}{K'}\right)^{\frac{1}{n'}} \end{cases}$$

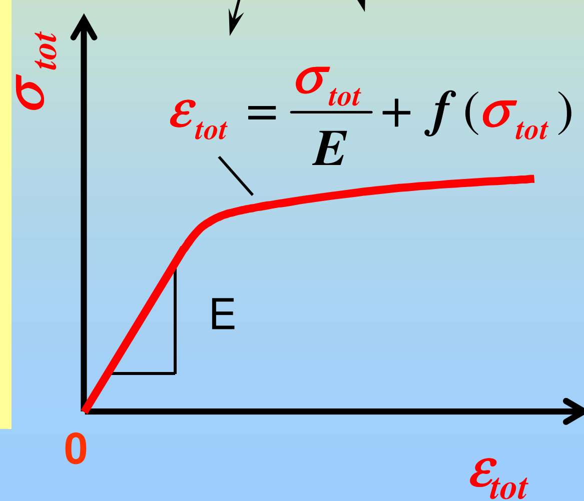

Equations of the multiaxial stresses and Hencky's equations of plasticity

$$
\begin{cases}
\varepsilon_{11}^{a} = \dfrac{1}{E}\left[\sigma_{11}^{a} - \nu\left(\sigma_{22}^{a} + \sigma_{33}^{a}\right)\right] - \dfrac{f(\sigma_{eq}^{a})}{\sigma_{eq}^{a}}\left[\sigma_{11}^{a} - \dfrac{1}{2}\left(\sigma_{22}^{a} + \sigma_{33}^{a}\right)\right] \\
\varepsilon_{22}^{a} = \dfrac{1}{E}\left[\sigma_{22}^{a} - \nu\left(\sigma_{33}^{a} + \sigma_{11}^{a}\right)\right] - \dfrac{f(\sigma_{eq}^{a})}{\sigma_{eq}^{a}}\left[\sigma_{22}^{a} - \dfrac{1}{2}\left(\sigma_{33}^{a} + \sigma_{11}^{a}\right)\right] \\
\varepsilon_{33}^{a} = \dfrac{1}{E}\left[\sigma_{33}^{a} - \nu\left(\sigma_{11}^{a} + \sigma_{22}^{a}\right)\right] - \dfrac{f(\sigma_{eq}^{a})}{\sigma_{eq}^{a}}\left[\sigma_{33}^{a} - \dfrac{1}{2}\left(\sigma_{11}^{a} + \sigma_{22}^{a}\right)\right] \\
\sigma_{11}^{e}\varepsilon_{11}^{e} = \sigma_{11}^{a}\varepsilon_{11}^{a} \\
\sigma_{22}^{e}\varepsilon_{22}^{e} = \sigma_{22}^{a}\varepsilon_{22}^{a} \\
\sigma_{33}^{e}\varepsilon_{33}^{e} = \sigma_{33}^{a}\varepsilon_{33}^{a}
\end{cases}
$$

$$
where: \; f(\sigma_{eq}^{a}) = \left(\frac{\sigma_{eq}^{a}}{K'}\right)^{\frac{1}{n'}}
$$

[A] , [B] and [D] are the elastic stiffness matrices derived by Tsai(1988):

$[A] = \int_h [C(x_3)]\, dx_3$, $[B] = \int_h [C(x_3)]\, x_3\, dx_3$ and $[D] = \int_h [C(x_3)]\, x_3^2\, dx_3$ (10)

$\vec{N}^*$ and $\vec{M}^*$ are the forces and moments respectively, generated by the eigenstrains $\varepsilon^*_{ij}(x_3)$

$$\vec{N}^* = \int_h [C(x_3)]\vec{\varepsilon}^*(x_3)dx_3 \quad \text{and} \quad \vec{M}^* = \int_h [C(x_3)]\vec{\varepsilon}^*(x_3)x_3 dx_3 \qquad (11)$$

From (8) and (9) we obtain:

$$\begin{pmatrix} \vec{N} + \vec{N}^* \\ \vec{M} + \vec{M}^* \end{pmatrix} = \begin{bmatrix} [A] & [B] \\ [B] & [D] \end{bmatrix} \begin{pmatrix} \vec{\varepsilon}^0 \\ \vec{k} \end{pmatrix} = [C'] \begin{pmatrix} \vec{\varepsilon}^0 \\ \vec{k} \end{pmatrix} \qquad (12)$$

Eq. (12) depicts 3 algebraic equations for $\vec{N}$ and three for $\vec{M}$ totaling 6 equations.

By inverting the matrix of these equation we solve with respect to the 6 components of ε_{ij}^0 and κ_{ij} :

$$\begin{pmatrix} \vec{\varepsilon}^0 \\ \vec{k} \end{pmatrix} = [C']^{-1} \begin{pmatrix} \vec{N} + \vec{N}^* \\ \vec{M} + \vec{M}^* \end{pmatrix}$$

Modulus and yield stress

The material properties used in this analysis are E = 116.3 GPa, ν = 0.349, K = 855 MPa, and n = 0.0149

The stress strain curve for Ti-6Al-4V alloy expressed by the Ramberg-Osgood equation:

$$\varepsilon = \frac{\sigma}{E} + \left(\frac{\sigma}{K}\right)^{\frac{1}{n}}$$

is depicted in Figure 8.

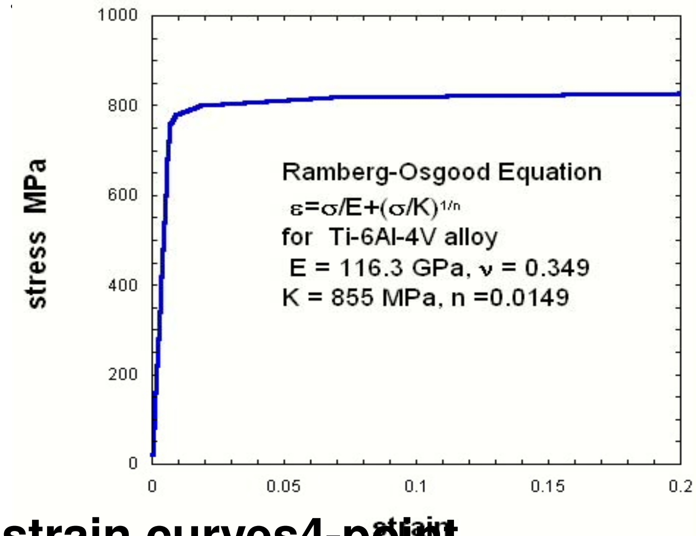

Experimental results from slopes of Bending versus strain curves4-point bending experiments the Elastic Modulus of Ti-6Al-4V substrate.

E'=137 GPa , E=117±3 GPa and yield stress σ_y=843 MPa

Literature: E=116.3±3 GPa, , σ_y=830 MPa $E_{coating}$ and K_{Ic} Fracture toughness, Tensile strength of Coating ~0,

Strain Mapping

ε_{11} depth (x_3) variation profiles of of alumina-titania-coating/Ti-substrate test specimen at various load levels in the four point bending geometry

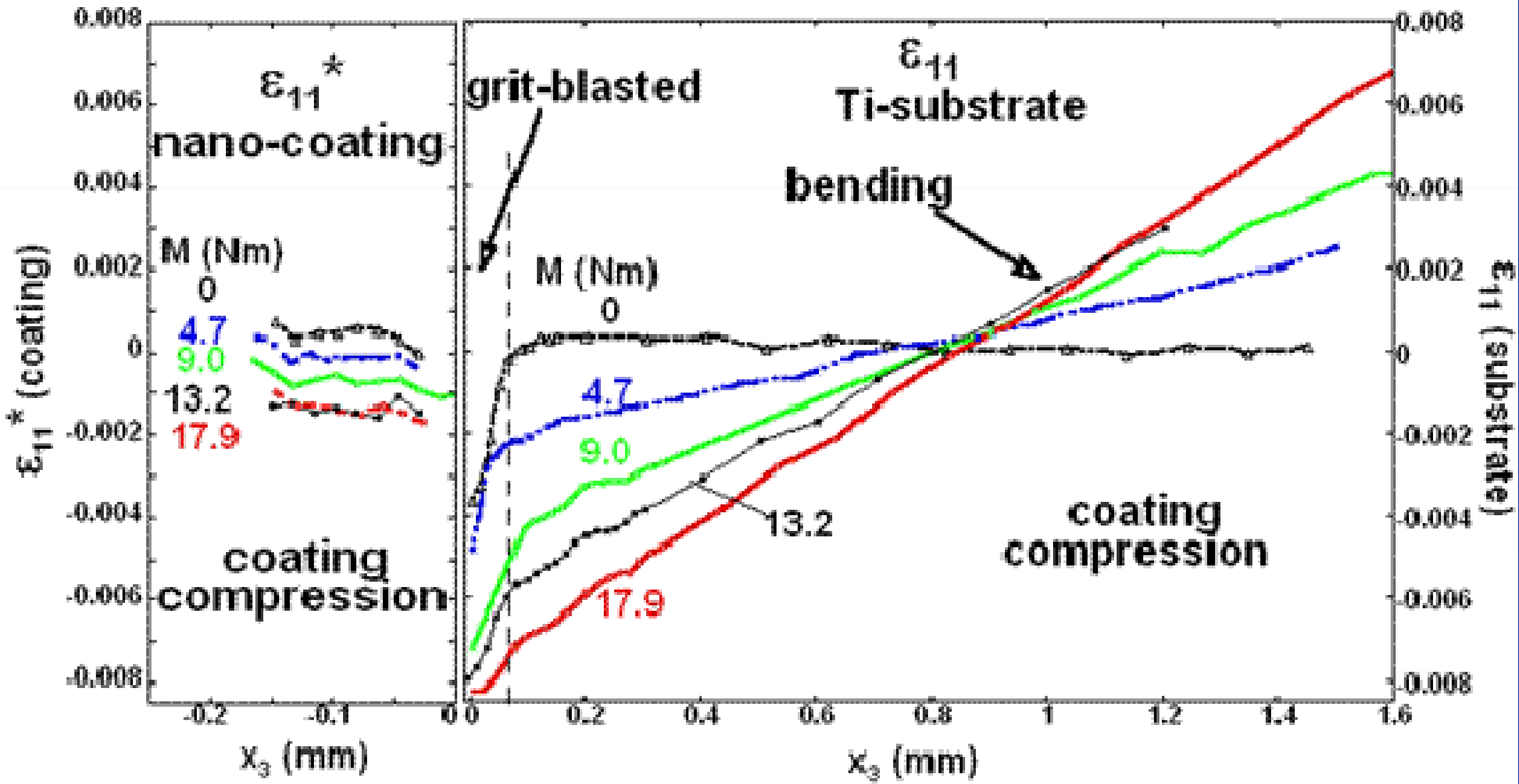

Phase Mapping

ε_{33} depth (x_3) variation profiles of of alumina-titania-coating/Ti-substrate test specimen at various load levels in the four point bending geometry.

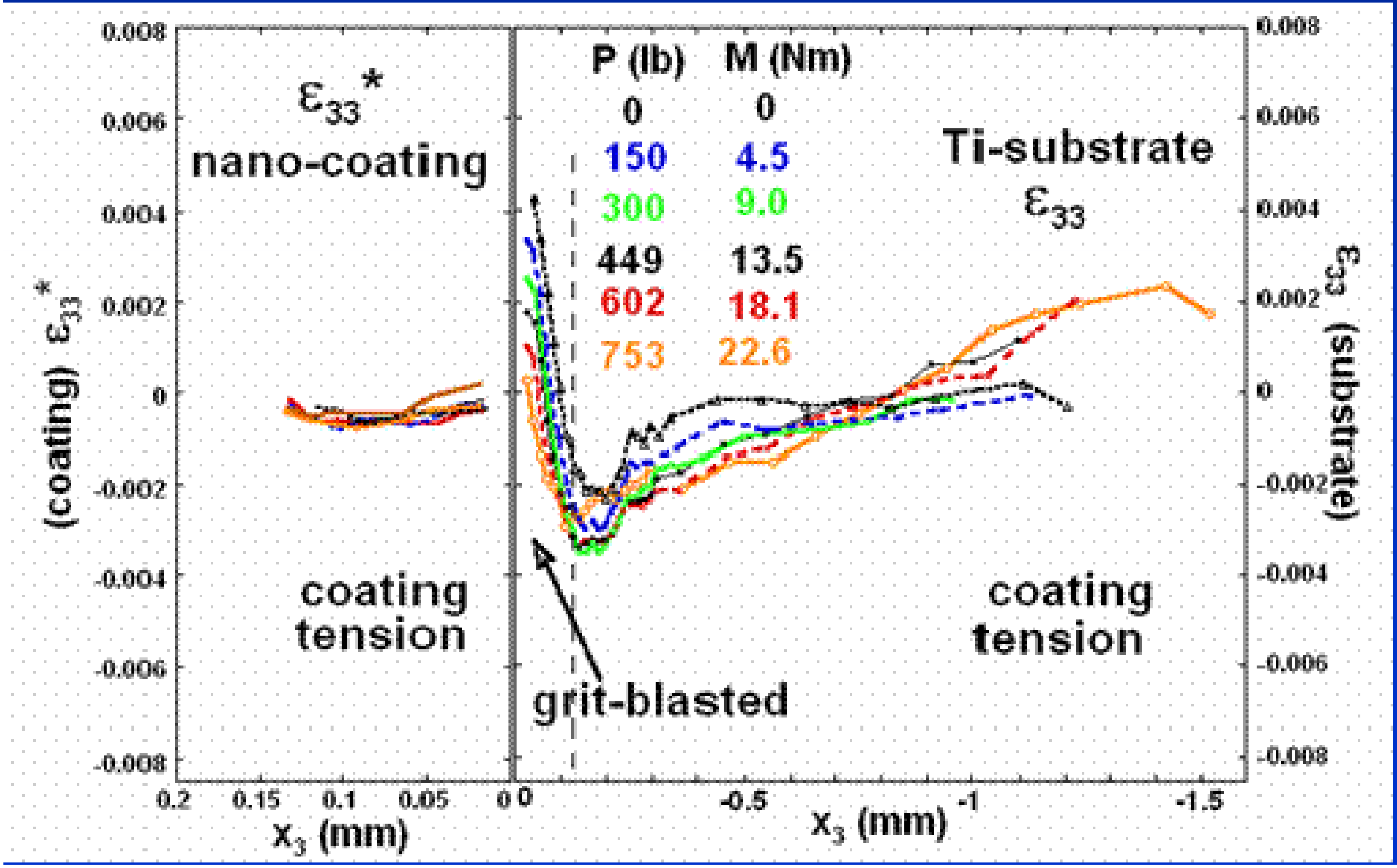

Modeling and Theory

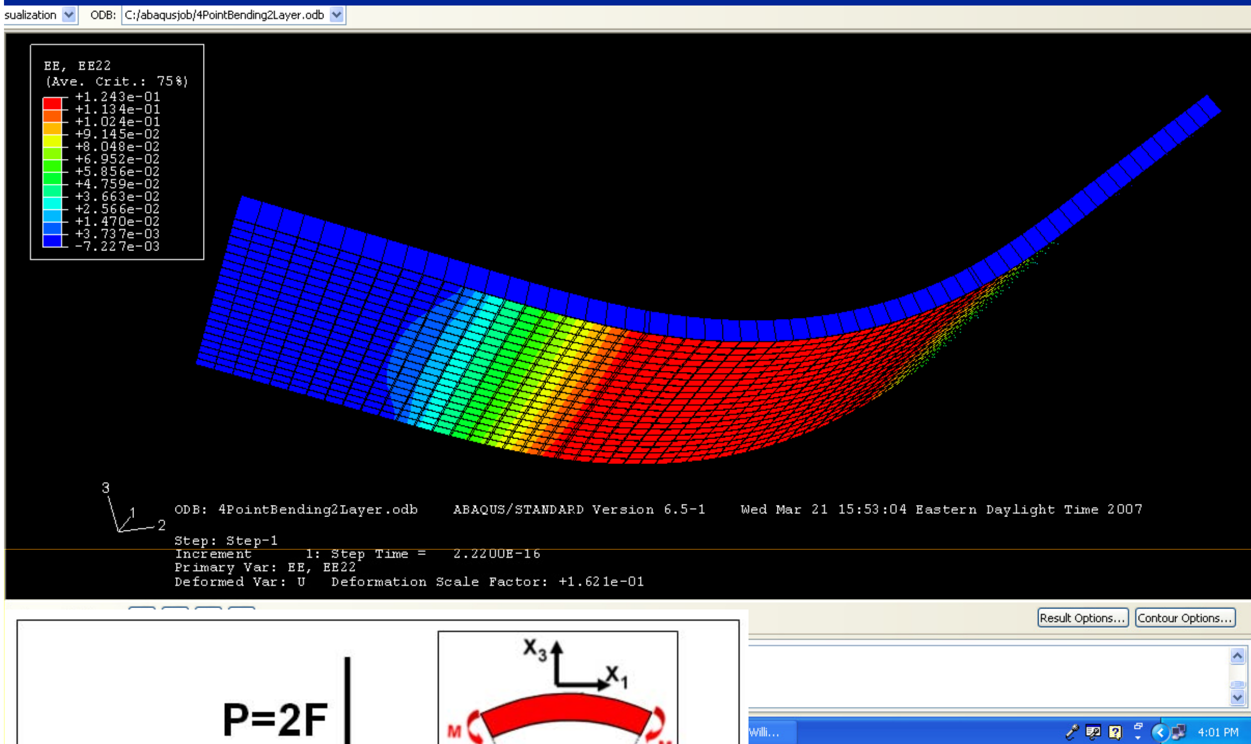

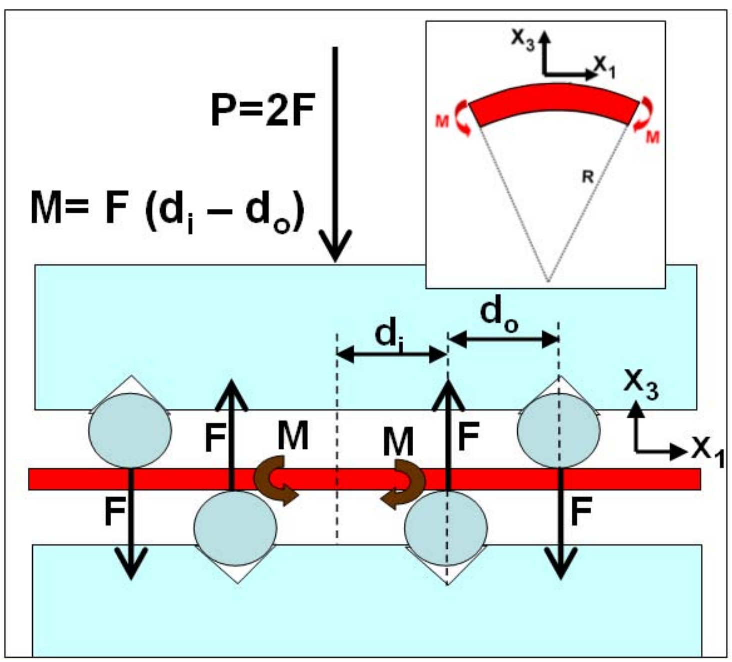

Energy Dispercsive X-ray Diffraction

Residual Stress

Macroscopic

- Non-destructive Measurements
- gauge evolution of RS
  for processing improvements
- validate FE Model

Microscopic

Micromechanisms of Deformation:

- Intergranular
- Interphase
- Phase Transformation

•Fracture toughness

Thank you.

Questions ?

A look to the future at EDXRD Residual Stress

- In-situ Synchrotron triaxial strain measurements
- Anisotropic materials
- Small strain systems
- Real time studies
- Small diffraction volumes (e.g. gradients, buried interfaces, grain boundaries,)
- Line Broadening studies

- Email tsakalak@rci.rutgers.edu

EDXRD Capabilities

Two themes (0-300 KeV photons)

a) High resolution Energy Dispersive X-ray Diffraction (EDXRD) 1 μm to 1 cm

b) High Energy EDXRD :Penetration depth ~ 2 inches of steel and 2 ft of Al

Two strategies

a) Strain Mapping (Internal/Residual Stress Spatial Distributions)

b) Phase Mapping (Spatial Distributions of Phases Stresses in each phase)

Three Scales:

a) Nanometer scale 0.1 to 100 nm (Line broadening EDXRD is best.

b) Mesoscopic scale 100 nm to 5 μm (individual grains, particles etc)

c) Macroscopic scale 5 μm to 10-100 mm

In situ Load/stress application (tensile, compressive, three point bending, etc load during measurement)

Performance studies in fatigue, fracture toughness, crack propagation, thermal shock stress effects and weldmends, shot $ laser peening, & other.

Measurement of microscopic stresses **within each phase** due to mismatch stresses and or thermal effects.

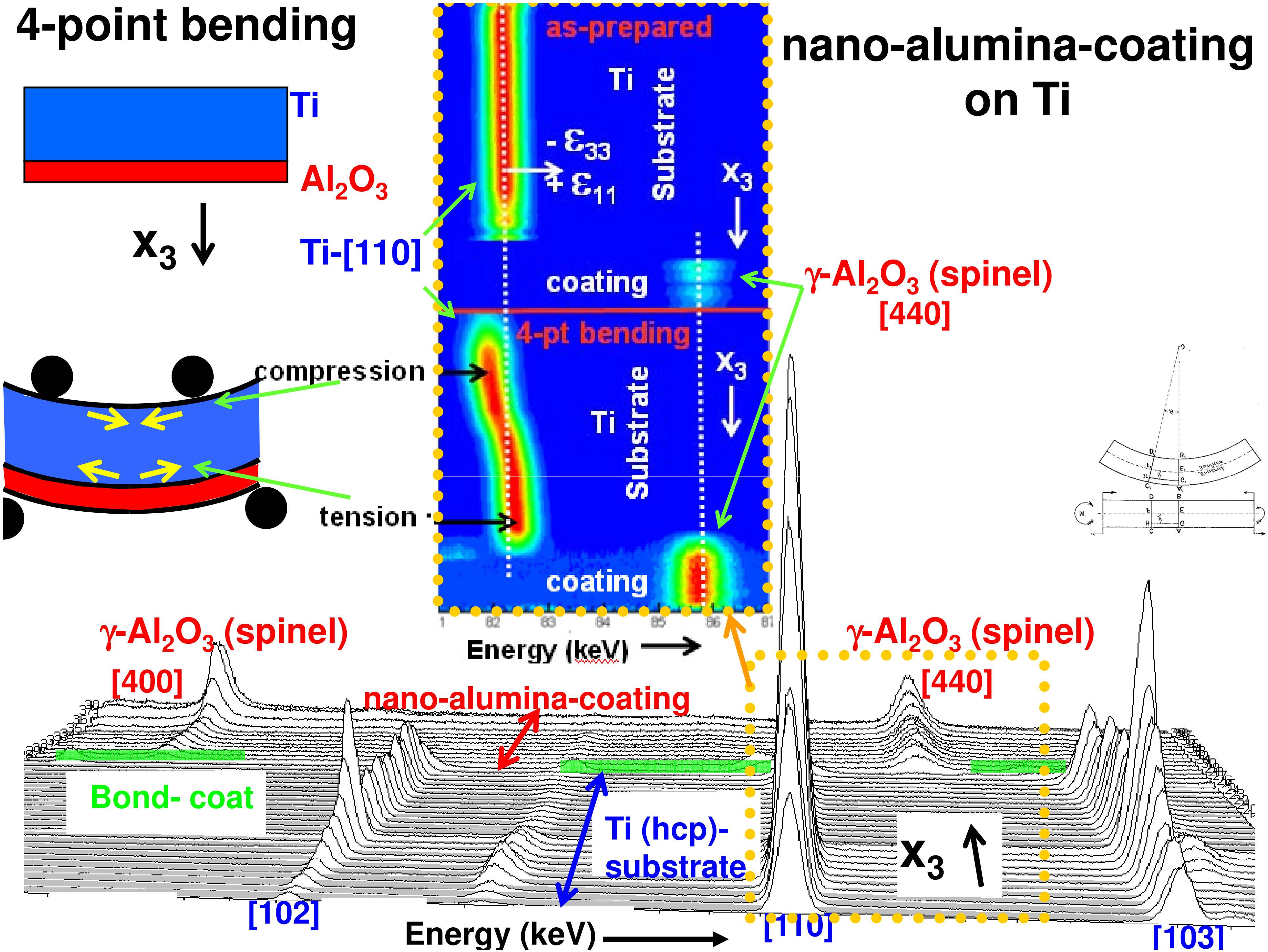
4-point bending
nano-alumina-coating on Ti
Ti
Al_2O_3
x_3
Ti-[110]
compression
tension
as-prepared
Ti
Substrate
$-\varepsilon_{33}$
$+\varepsilon_{11}$
x_3
coating
4-pt bending
x_3
Ti
Substrate
coating
Energy (keV)
γ-Al_2O_3 (spinel)
[440]
γ-Al_2O_3 (spinel)
[400]
nano-alumina-coating
γ-Al_2O_3 (spinel)
[440]
Bond- coat
Ti (hcp)-
substrate
x_3
[102]
Energy (keV)
[110]
[103]

Complex strain regimes

nano-alumina-coating on Ti

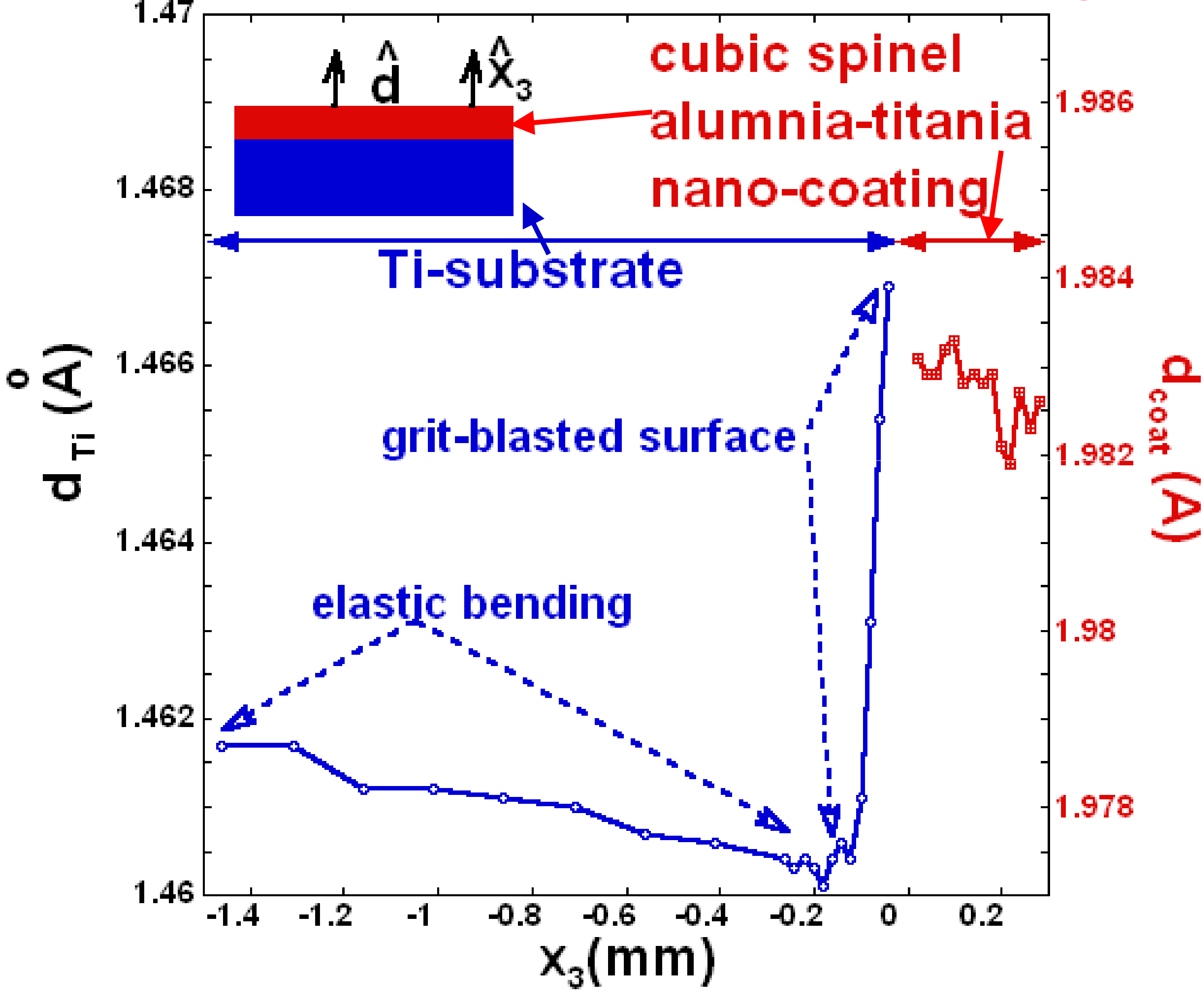

Modeling and Theory

$$\sigma_{11} = \frac{E\varepsilon_{11}}{1-\nu^2} = -\frac{Ex_3}{1-\nu^2}\frac{d^2 v_3}{dx_1^{\ 2}} = \frac{Ex_3}{1-\nu^2}\kappa_{11}$$

Integrating over cross section area we obtain the moment

$$M = -\int_h \sigma_{11} L_2 x_3 dx_3 = \left(\frac{EI}{1-\nu^2}\right)\frac{d^2 v_3}{dx_1^{\ 2}} = E'I\kappa_{11}$$

Where $E' = \dfrac{E}{1-\nu^2}$ and $I = \dfrac{L_2 h^3}{12}$

The transverse strain $\varepsilon_{33}=(1/E)(-\nu(\sigma_{11}+\sigma_{22}))=-\nu(1+\nu)\sigma_{11}=[-\nu/(1-\nu)]\ \varepsilon_{11}$

$\varepsilon_{33}=[-\nu/(1-\nu)]\ \varepsilon_{11}$

For $\nu=1/3$, $\varepsilon_{33}=-(1/2)\ \varepsilon_{11}$

Micromechanics and Kirchoff's formalism of multilayers.

For such loading, we can neglect the transverse components of the strain ε_{3i}. Large deformations have not been employed here due to the small thickness. In the context of micromechanics the elastic strain tensor ε^{el}_{ij} is given by:

$$\varepsilon^{el}_{ij}(x_3)=\varepsilon^{tot}_{ij}(x_3)-\varepsilon^{*}_{ij}(x_3) \quad (1)$$

where the total strain from classical Kirchoff plate theory is given by:

$$\varepsilon^{tot}_{ij}(x_3)=\varepsilon^{0}_{ij}+\kappa_{ij}\, x_3 \quad (2)$$

where **the curvatures κ_{ij} and the strains ε^{0}_{ij} at $x_3 = 0$ can be assumed to be constant** in the plate and i, j indices take values 1, 2 (in plane stresses case).

From micromechanics the constitutive equation can be written as:

$$\sigma_{ij}(x_3)=[C_{ijkl}](\varepsilon^{tot}_{kl}-\varepsilon^{*}_{kl}) \quad (3)$$

where C_{ijkl} represent the general stiffness matrix for the in plane stress-strain tensor case. From Eqs. (2) and (3) we can obtain the resultant force and moment due to the stress distribution in the x_3 through the thickness of our plate.

$$N_{ij}=\int_h \sigma_{ij}(x_3)\, dx_3 \qquad \text{and} \qquad M_{ij}=\int_h \sigma_{ij}(x_3)\, x_3\, dx_3$$